NOVA SCHOOL OF SCIENCE & TECHNOLOGY

DEPARTAMENT OF
Chemistry

Diogo dos Santos Feliciano de Sousa Ventura
BSc in Biology

Pilot-Scale Production of PHA from Apple Pulp Waste: Impact of Purge Timing and Feeding Strategy

MASTER IN BIOENERGY AND SUSTAINABLE TECHNOLOGIES
NOVA University Lisbon
September, 2025

NOVA SCHOOL OF SCIENCE & TECHNOLOGY

DEPARTAMENT OF
Chemistry

Pilot-Scale Production of PHA from Apple Pulp Waste: Impact of Purge Timing and Feeding Strategy

Diogo dos Santos Feliciano de Sousa Ventura

BSc in Biology

Adviser: Nídia Dana Mariano Lourenço
Auxiliary Professor, NOVA University Lisbon, Portugal

Co-advisers: Mariana Campos de Matos
Auxiliary Researcher, NOVA University Lisbon, Portugal

Examination Committee:

Chair: Professor Doctor Nuno Carlos Lapa dos Santos Nunes,
Auxiliary Professor, NOVA University Lisbon

Rapporteurs: Professor Doctor Maria Teresa Cesário Smolders,
Auxiliary Researcher, University of Lisbon

Adviser: Professor Doctor Nídia Dana Mariano Lourenço,
Auxiliary Professor, NOVA University Lisbon

MASTER IN MSC BIOENERGY AND SUSTAINABLE TECHNOLOGIES

NOVA University Lisbon
September, 2025

Pilot-Scale Production of PHA from Apple Pulp Waste: Impact of Purge Timing and Feeding Strategy

Declaration of AI usage

In this work, generative artificial intelligence tools were used, namely Perplexity Pro (https://www.perplexity.ai/), for grammar review and text reformulation. These tools were used under the supervision of the author, and all generated content was checked for accuracy. The authorship and validation of the content remain entirely the responsibility of the author, and the use of artificial intelligence is in accordance with institutional standards of academic integrity.

For my grandparents.

ACKNOWLEDGMENTS

This study was funded by the European Commission within the program HORIZON EUROPE in the framework of the UPSTREAM project (HORIZON-MISS-2022-OCEAN-01-04-101112877), and by national funds from FCT - Fundação para a Ciência e a Tecnologia, I.P., in the scope of the project UIDP/04378/2020 and UIDB/04378/2020 of the Research Unit on Applied Molecular Biosciences - UCIBIO, and the project LA/P/0140/2020 of the Associate Laboratory Institute for Health and Bioeconomy - i4HB.

This thesis marks the end of a very good phase. It was full of great, and not so great, moments that helped shape the way I am. All the small victories and small lessons contributed in one way or another to the person I turned out to be.

First of all, I want to thank Prof. Dr. Nídia Lourenço and Dr. Mariana Matos for giving me the chance to participate in this project, I hope I was able to properly justify your bet on me. A special thanks to Dr. Mariana Matos for all the patience to discuss my every question.

I'd like to thank Dr. Eliana Guarda and Dr. João Pereira for all the guidance, advice and friendship given throughout this year. You are probably the reason why I finished my thesis without some permanent disability. I hope I was able to somehow give something back besides headaches and loss of sleep.

A thank you to Elsa Mora Mestre for all the samples analyzed, I'm sorry for the hundreds you had to analyze through the year and thank you for always trying to facilitate my work.

Marisa Saloio and Jorge Viana, thank you for all the help you gave in the lab. After all this time I am confident that we developed a good friendship while working. Marisa, I am very happy for you for entering in a doctoral program, I am sure that you will be able to make a very thesis. Jorge, you are halfway done with your doctorate, I hope the rest of your program goes as easily it was until now, you have a special way of always making things look very easy and doable.

To Marta Rodrigues and Cláudia Duarte, I am especially grateful for always bringing the good vibes to the lab. You were always able to lift the mood of the room even when accidents happened. Hope the writing of your theses goes as well as mine.

Despite leaving, I recognise and am thankful for what Marisa Cardoso thought me about the UASB reactor, and we actually had some good laughs during her stay in the pilot lab.

I want to thank my family. Thank you to my parents, José and Vera, for always believing in my capabilities, even when I did not, and for investing in my education while providing everything I could need to prosper and thrive. Thanks to my brother David for always being present and providing support that most of the times you didn't even notice you were giving. Thaks to my grandparents, Joaquim and Noémia, for always doing way more than what was required, you are a big part of the way I am, and I appreciate you more than you realise.

Thank you to my amazing girlfriend Catarina for all of the support given. Since we met you were always a safe space for me and through the years you always went above and beyond to help and make me happy. You really changed me for the better and I am thankful every day for having you in my corner.

"Last but not least, I want to thank me. I want to thank me for believing in me. I want to thank me for doing all this hard work. I want to thank me for having no days off. I want to thank me for never quitting. I want to thank me for always being a giver, and trying to give more than I receive. I want to thank me for trying to do more right than wrong. I want to thank me for just being me at all time."

"Either I will find a way or I will make one." (Hannibal Barca).

ABSTRACT

Polyhydroxyalkanoates (PHAs) are bioplastics produced by microorganisms, with properties similar to those of conventional plastics, but with less environmental impact. Their innovative production uses mixed microbial cultures (MMCs) fed with waste, divided into three stages: (i) acidogenesis of the substrate, (ii) microbial selection in a sequencing batch reactor (SBR) under conditions of feast/famine, and (iii) accumulation in a reactor, where high PHA contents are achieved. This last stage is an obstacle due to high carbon requirements and costs. The objective of this work was to develop strategies to maximize productivity and polymer content, reducing or avoiding accumulation. Two approaches were tested: purging the SBR after feast to obtain biomass richer in PHA or purging after feast with doubling of the organic load, comparing them to the traditional strategy of purging after famine.

The first strategy proved the most effective, it increased biomass productivity (1.66 ± 0.02 vs. 1.3 ± 0.1 g-X_a/(L·d) in the traditional strategy), global PHA productivity (1.47 ± 0.2 vs. 1.18 ± 0.01 g-PHA/(L·d)), and global yield (0.30 vs. 0.19 g-COD_{PHA}/g-COD_{FPs}). This allowed the SBR to be purged with biomass richer in PHA without compromising biomass productivity, leading to a more efficient process.

In contrast, the two-pulse feast strategy required substantially higher carbon input in the SBR to increase PHA content. Although biomass productivity increased (2.09 ± 0.04 g-X_a/(L·d)), global yield decreased (0.21 g-COD_{PHA}/g-COD_{FPs}), since the additional carbon consumed for biomass growth did not compensate for the benefits of reducing the need for an accumulation reactor.

In conclusion, the purging after feast strategy constitutes a more sustainable and cost-effective alternative to the conventional process, reducing carbon consumption and minimizing the need for a separate accumulation stage.

Keywords: polyhydroxyalkanoates (PHA), Mixed Microbial Cultures (MMCs), purging strategy, feeding strategy, performance optimization

RESUMO

Os polihidroxialcanoatos (PHAs) são bioplásticos produzidos por microrganismos, com propriedades semelhantes às dos plásticos convencionais, mas menor impacto ambiental. A sua produção inovadora usa culturas microbianas mistas (MMCs) alimentadas com resíduos, dividindo-se em três etapas: (i) acidogénese do substrato, (ii) seleção microbiana num *sequencing batch reactor* (SBR) sob condições de abundância/escassez e (iii) acumulação num reator, onde se atingem altos teores de PHA. Esta última etapa constitui um entrave devido à elevada exigência de carbono e custos. O objetivo deste trabalho foi desenvolver estratégias para maximizar produtividade e teor de polímero, reduzindo ou evitando a acumulação. Foram testadas duas abordagens: purgar o SBR após a abundância para obter biomassa mais rica em PHA ou purgar após abundância com duplicação da carga orgânica, comparando-as à estratégia tradicional de purgar após a escassez.

A primeira estratégia provou ser a mais eficaz, aumentando a produtividade da biomassa (1.66 ± 0.02 vs. 1.3 ± 0.1 g-X_a/(L·d) na estratégia tradicional), a produtividade global de PHA (1.47 ± 0.2 vs. 1.18 ± 0.01 g-PHA/(L·d)) e o rendimento global (0.30 vs. 0.19 g-COD_{PHA}/g-COD_{FPs}). Isto permitiu purgar o SBR com biomassa mais rica em PHA sem comprometer a produtividade da biomassa, levando a um processo mais eficiente.

Em contrapartida, a estratégia de dois pulsos exigiu uma entrada substancialmente maior de carbono no SBR para aumentar o teor de PHA. Embora a produtividade da biomassa tenha aumentado (2.09 ± 0.04 g-X_a/(L·d)), o rendimento global diminuiu (0.21 g-COD_{PHA}/g-COD_{FPs}), uma vez que o carbono adicional consumido para o crescimento da biomassa não compensou os benefícios da redução da necessidade de um reator de acumulação.

Em conclusão, a estratégia de purga após a abundância constitui uma alternativa mais sustentável e económica ao processo convencional, reduzindo o consumo de carbono e minimizando a necessidade de uma fase de acumulação separada.

Palavras chave: polihidroxialcanoatos (PHA), culturas microbianas mistas (MMCs), estratégia de purga, estratégia de alimentação, otimização de desempenho

CONTENTS

LIST OF FIGURES

LIST OF TABLES

ACRONYMS

(-) q_{FP}	Substrate Uptake Rate
(-) q_{PHA}	PHA Consumption During Famine
COD	Chemical Oxygen Demand
$Đ_M$	Dispersity
DO	Dissolved Oxygen
DSC	Differential Scanning Calorimetry
E	Young's Module
F/F	Feast-Famine
F/M	Food-Microorganism
FPs	Fermentation Products
GAO	Glycogen Accumulation Organisms
GC	Gas Chromatography
HB	3-hydroxybutyrate
HHx	3-hydroxyhexanoate
HRT	Hydraulic Retention Time
HV	3-hydroxyvalerate
MMC	Mixed Microbial Cultures
M_n	Number of Molecular Weights

M_W	Average of Molecular Weights
N&P	Nitrogen and Phosphorous
OLR	Organic Loading Rate
PHA	Polyhydroxyalkanoate
PHB	Poly(3-hydroxybutyrate)
PHBV	Poly(3-hydroxybutyrate-co-3-hydroxyvalerate)
q_{PHA}	PHA Accumulation Rate
q_{Xa}	Maximum Specific Growth Rate
rPHA	PHA Productivity During Accumulations
SBR	Sequencing Batch Reactor
SRT	Sludge Retention Time
T_c	Melt Crystallization Temperature
T_{cc}	Cold Crystallization Temperature
T_{deg}	Temperature of 5% Degradation
T_g	Glass Transition Temperature
TGA	Thermo-Gravimetric Analysis
T_m	Melting Point
TSS	Total Suspended Solids
UASB	Upflow Anaerobic Sludge Blanket
UTS	Ultimate Tensile Strength
VFA	Volatile Fatty Acid
VSS	Volatile Suspended Solids
X_a	Active Biomass
XPR	Biomass Volumetric Productivity
$Y_{X/PHA}$	Growth Yield in Famine

Δ_m	Melting Enthalpy
ε	Elongation at Break

1 INTRODUCTION

1.1 Climate change, plastics and its impact on the environment

In the contemporary global context, dependency on coal, oil, and natural gas persists despite substantial evidence regarding their adverse climatic impacts. This dependence engenders geopolitical vulnerability, economic instability, and potential future scarcity, as easily exploitable reserves decline and prices fluctuate in response to market and regulatory changes. (Achakulwisut et al., 2023; Mohamued et al., 2021; Neofytou et al., 2018). Annual fossil fuel consumption exceeds 11 billion metric tons, primarily driven by energy, manufacturing, and transportation sectors, resulting in considerable carbon dioxide (CO_2) emissions, the principal greenhouse gas, elevating atmospheric concentrations to historic levels, intensifying global warming, and exacerbating the frequency and severity of extreme weather events such as droughts, floods, and hurricanes (Sergeant, 2024; Yang et al., 2023; Ye, 2024; Yusuf & Abdullah, 2020).

Beyond combustion, fossil fuel derivatives underpin the production of fuels and plastics. These materials are ubiquitous in modern society, however, improper disposal causes significant environmental and health harms. Plastics accumulate within terrestrial and marine ecosystems, enter food webs, and have been detected in human tissues (Achakulwisut et al., 2023; Lelieveld et al., 2023). Preliminary evidence correlates this pollution with increased risk of inflammatory, neurodegenerative, and metabolic diseases, underscoring the urgent necessity for reformed production, consumption, and waste management practices (Maurya et al., 2021; Sergeant, 2024; Ye, 2024).

1.2 Plastics

Plastics can originate from both fossil fuels and renewable biological sources, each with distinct environmental and economic implications (Jiang et al., 2024; Rhodes, 2018) (**Figure 1.1**). Fossil-based plastics dominate global production, while bioplastics are emerging as a

more sustainable alternative (Rhodes, 2018). Comparing their properties, applications, and impacts is essential to understanding their role in a circular economy.

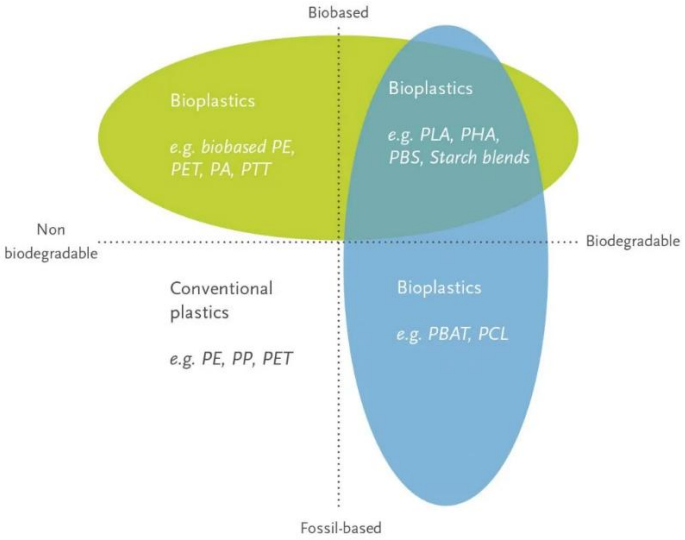

Figure 1.1-Graphic of the classification of plastics based on Bio/Fossil- based and biodegradability (*What Is the Difference between Biobased and Biodegradable Plastics? – INGREEN, n.d.).*

1.2.1 Fossil-fuel based

Fossil-fuel based plastics are synthetic polymers produced primarily from hydrocarbons derived from the refining and steam cracking of crude oil and natural gas, which generate key monomers like ethylene, propylene, and styrene that are polymerized via catalytic reactions to form materials such as polyethylene, polypropylene, and polystyrene (Achakulwisut et al., 2023; Maurya et al., 2021; Schernikau & Smith, 2022; Ye, 2024). Although these plastics are economically versatile, their exclusive reliance on finite fossil feedstocks exacerbates resource depletion and carbon emissions, while their environmental persistence is reflected in their resistance to biodegradation, resulting in the accumulation of macroplastics, microplastics, and nanoplastics in ecosystems, which disrupts nutrient cycles and endangers both wildlife and human health by bioaccumulation (Achakulwisut et al., 2023; Lelieveld et al., 2023; Maurya et al., 2021; Sergeant, 2024).

1.2.2 Bioplastics

Bioplastics are a diverse class of polymeric materials designed as environmentally responsible alternatives to conventional plastics, distinguished by both their origins, usually renewable biological resources, and their functional attributes, such as biodegradability (Costa et al., 2023; Kshirsagar et al., 2023; Mukherjee et al., 2023). These materials are typically

synthesized from plant-derived sugars, starches, vegetable oils, or agricultural byproducts, making them fundamentally renewable and helping lower carbon emissions across their lifecycle (Costa et al., 2023; Mukherjee et al., 2023).

Not all bioplastics are biodegradable, but many are engineered to degrade via microbial action into water, CO_2, and biomass under controlled conditions, reducing their long-term environmental impact compared to fossil plastics (Costa et al., 2023; R. M. S. Cruz et al., 2022; Folino et al., 2020). Examples like polylactic acid (PLA), polyhydroxyalkanoates (PHA), and blended polymers such as polybutylene adipate terephthalate (PBAT) showcase varying combinations of biobased origin and biodegradability, underpinning their integration into circular economy models focused on composting, recycling, and transformation of waste into high-value products (Costa et al., 2023; Gontard et al., 2022; Mukherjee et al., 2023; Tábi, 2022).

1.2.2.1 Polyhydroxyalkanoates

PHAs are a family of biopolyesters synthesized by a variety of bacterial species as intracellular carbon and energy storage compounds, particularly under conditions where nutrients such as nitrogen or phosphorus are limited and carbon sources are in excess (Guzik, 2021; Koller, 2018; Thorat Gadgil et al., 2017). These bioplastics are gaining global attention due to their inherent biodegradability, renewability, and biocompatibility, features that make them attractive substitutes for petroleum-derived polymers in both industrial and medical contexts (Guzik, 2021; Koller, 2018). Chemically, PHAs consist of repeating hydroxyalkanoate units, with a general formula of $[–O–CHR–CH_2–CO–]_n$, where "R" represents a variable sidechain. This sidechain determines the specific monomer type, ranging most commonly from methyl groups (as in 3-hydroxybutyrate, HB), ethyl groups (in 3-hydroxyvalerate, HV), to longer aliphatic chains (such as in 3-hydroxyhexanoate, HHx) (Koller, 2018; Thorat Gadgil et al., 2017). The nature and ratio of these monomers, whether incorporated singly or as copolymers, play a crucial role in dictating the physical and mechanical properties of the resulting polymer. For instance, pure polyhydroxybutyrate (PHB) is known to be highly crystalline, stiff, and brittle, suitable for rigid packaging uses. By introducing hydroxyvalerate or hydroxyhexanoate units (forming PHBV or PHBHHx copolymers), the polymer becomes notably more flexible and elastic, with diminished crystallinity and enhanced impact resistance (Koller, 2018; Thorat Gadgil et al., 2017). The structure of the most common PHAs can be found in **Figure 1.2**.

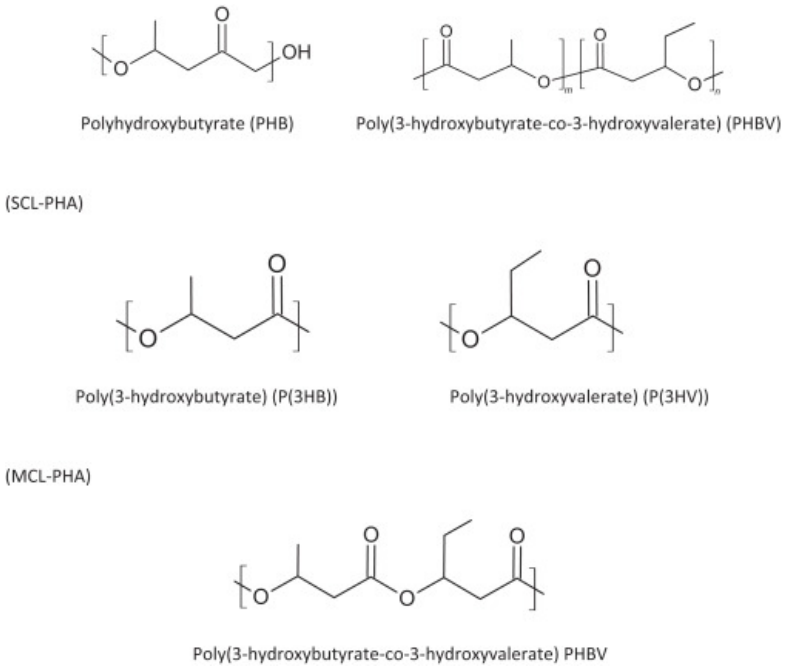

Figure 1.2-Structure of the most common PHAs.

The biosynthesis of PHAs in microorganisms proceeds through distinct metabolic pathways depending on the substrate and organism involved. Typically, simple sugars or fatty acids are processed via central metabolic routes: carbohydrates feed into the acetyl-CoA pathway for HB production, while propionate or valerate sources yield HV monomers through propionyl-CoA intermediates (Guzik, 2021; Mittendorf et al., 1998). Fatty acids, especially in certain *Pseudomonas* and *Aeromonas* species, are funneled into the β-oxidation cycle which allows the synthesis of medium- and long-chain-length PHAs (e.g., HHx) (Guzik, 2021; Mittendorf et al., 1998). All routes eventually generate hydroxyacyl-CoA thioesters, which are polymerized by intracellular PHA synthase enzymes into high-molecular-weight polymers that precipitate as granules within the cell's cytoplasm. These granules, whose physical state and molecular weight are shaped by microbial genetics and fermentation conditions, are then extracted for various practical uses (Guzik, 2021; Mittendorf et al., 1998; Thorat Gadgil et al., 2017).

Monomer composition, especially the ratios of HB, HV, and HHx, impart dramatic variation in the mechanical and thermal behavior of PHAs. Increasing the proportion of HV in PHBV copolymers decreases crystallinity and brittleness, produces softer, more flexible materials, and increases the ease of processing and application in flexible films and bags (Koller, 2018; Maestro & Sanz, 2017). When HHx is incorporated, especially at higher ratios, the polymer exhibits even greater elasticity and toughness, making it an ideal candidate for elastic films, soft biomedical implants, and applications requiring enhanced resistance to dynamic

forces (Barbosa et al., 2021; Lidón Sánchez-Safont et al., 2016). Molecular weight further modulates these attributes: higher molecular weights confer improved processability and strength (Koller, 2018; Maestro & Sanz, 2017).

PHAs have found burgeoning applications in both packaging and biomedical sectors; in packaging, they are used for compostable bags, wrappers, and agricultural films, while in medicine, their biocompatibility and degradation to harmless hydroxy acids allow uses in absorbable sutures, scaffolds, patches, and drug delivery systems (Getino et al., 2024; Guzik, 2021; Kalia et al., 2023; Koller, 2018; Roman et al., 2020). The ability to tailor PHA properties by manipulating monomer inclusion during biosynthesis enables the design of materials that meet rigorous physical, chemical, and biological specifications, establishing PHAs as promising candidates for sustainable manufacturing and advanced biomedical technology (Getino et al., 2024; Kalia et al., 2023).

1.3 PHA production

PHA production represents a pivotal advancement in the pursuit of sustainable bioplastics, relying on the capacity of microorganisms to synthesize and store these biodegradable polyesters as intracellular granules. Industrial approaches to PHA biosynthesis generally employ either pure microbial cultures, selected and cultivated under sterile, tightly controlled conditions for optimal yield and polymer quality, or mixed microbial cultures (MMCs), which leverage the metabolic versatility of diverse consortia to valorize organic wastes in open, non-sterile systems (Bagatella et al., 2022; Morgan-Sagastume, 2016). The choice between pure and mixed culture methodologies decisively shapes process economics, substrate adaptability, and end-product properties, underscoring the need to assess both systems relative advantages, challenges, and technological implications for scalable and eco-friendly biopolymer production (Bagatella et al., 2022; Morgan-Sagastume, 2016).

1.3.1 Pure cultures

The production of PHAs via pure bacterial cultures is one of the leading methods in industrial biotechnology, employing single strains like *Cupriavidus necator*, *Alcaligenes latus* or various *Pseudomonas spp*. for their robust capacity to synthesize and accumulate PHAs intracellularly under specific culture regimens (Getino et al., 2024; Kalia et al., 2025; Wongsirichot, 2025). These microbes are grown in sterile bioreactors supplied with renewable carbon sources, and after reaching a target biomass, a nutrient limitation (usually nitrogen or phosphorus) is

imposed while carbon remains in excess, inducing polymer accumulation as granules that can reach up to 80% of the cell's dry weight in optimal conditions (Kalia et al., 2025; Wongsirichot, 2025).

Following accumulation, bacterial cells undergo harvesting and downstream processing, which involves extraction and purification of the intracellular PHAs via chemical or enzymatic methods tailored for integrity and control over molecular characteristics (Getino et al., 2024). The high purity and compositional precision enabled by pure culture systems yield materials with predictable mechanical and thermal properties, crucial when polymers are destined for food packaging or biomedical applications requiring strict quality specifications (Getino et al., 2024).

Despite their significant advantages in terms of material quality and process control, pure culture systems are limited by high operational costs, stemming from sterile conditions, expensive substrates, and complex bioreactors, as well as fluctuating substrate availability and sensitivity to operational parameters like temperature, pH, and oxygen (Getino et al., 2024; Kalia et al., 2025; Wongsirichot, 2025). Nevertheless, modern approaches in strain engineering, fermentation technology, and sustainable feedstock utilization continue to push the economic and environmental viability of pure culture PHA production, establishing it as essential for future biodegradable polymer manufacturing (Getino et al., 2024; Kalia et al., 2025; Wongsirichot, 2025).

1.3.2 Mixed microbial cultures (MMC)

The production of PHAs using MMCs has emerged as a cost-effective and resource-efficient alternative to pure culture systems, especially for applications involving waste valorization and integration into circular economy frameworks. The MMC-driven PHA production process typically encompasses two key stages: an initial enrichment phase where microbial communities are subjected to periodic feeding of volatile fatty acids (VFAs), such as acetic, butyric and valeric acids, under "feast–famine" conditions, favoring the selection of microorganisms capable of efficiently storing PHAs; followed by a subsequent accumulation phase, where the selected biomass is exposed to excess VFAs under nutrient-limited conditions, promoting maximum polymer synthesis within the cells (Alfano et al., 2021; Bagatella et al., 2022). Commonly, the enrichment is carried out in sequencing batch reactors (SBRs) where parameters like aeration rate (which can significantly affect both microbial selection and PHA yields), organic loading rate (OLR), and hydraulic retention time (HRT) are tightly controlled (Bagatella

et al., 2022; Colombo et al., 2017). The substrate sources for MMC processes are notably varied, ranging from fermented agrifood waste or cheese whey to fermented wastewater sludge or lignocellulosic biomass, all providing mixed VFAs as the main carbon and energy source for PHA synthesis (Bravo-Porras et al., 2024; Castagnoli et al., 2024). The resulting polymers are often copolymers, like PHBV, whose composition and molecular weight depend heavily on the feedstock's VFA profile and microbial community structure (Alfano et al., 2024). Downstream, the recovery of PHAs from MMC-grown biomass often relies on chemical digestion (e.g., sodium hydroxide or hypochlorite treatments) or greener solvents such as ethyl acetate, with process optimization paramount to balancing purity, yield, and cost (Alfano et al., 2021; Bagatella et al., 2022; Castagnoli et al., 2024; Colombo et al., 2017).

MMCs systems have significant advantages that underpin their growing adoption. First and foremost, they eliminate the need for costly sterilization, operations can be run in open, non-sterile environments, greatly reducing capital and operational expenditure (Afreen et al., 2021). Additionally, MMCs offer versatility in substrate utilization, with the ability to valorize low-value, heterogeneous waste streams (e.g., food waste, municipal sludge) into high-value biopolymers, thereby integrating waste management with sustainable materials production (Afreen et al., 2021; Bagatella et al., 2022). The flexibility in community adaptation and metabolic pathways enables MMC processes to cope with the complexity of real waste streams, as opposed to the strict substrate needs of pure culture systems(Bedade et al., 2021). MMC-based PHA production is thus increasingly viewed as a cornerstone technology for circular bioeconomy frameworks, enabling the reduction of environmental “white pollution” and advancement toward global sustainability goals (Afreen et al., 2021; Bedade et al., 2021).

1.3.3 Three-stage process

The three-stage process for PHA production with MMCs segments the workflow into feedstock fermentation, microbial enrichment, and accumulation phases. First, organic wastes are anaerobically fermented to generate VFAs, which serve as primary carbon sources for later microbial growth (Bagatella et al., 2022). In the second stage, feast and famine cycles in sequencing batch reactors select for microbes capable of quickly taking up VFAs and storing them as PHA granules (Bravo-Porras et al., 2024; Duque et al., 2014). The final stage involves feeding this enriched biomass with VFA-rich substrates under nutrient-limited conditions to maximize intracellular PHA accumulation (Valentino et al., 2015). This approach enhances

process control, yield, and product tailoring, making it well-suited to the use of diverse, low-cost waste streams.

1.3.3.1 Acidogenic Reactor

The acidogenic reactor is the critical first step in the three-stage process for PHA production with MMCs, functioning primarily to convert complex organic waste substrates into a spectrum of VFAs that serve as key precursors for downstream PHA synthesis (Albuquerque et al., 2010). In this stage, Upflow Anaerobic Sludge Blanket (UASB) bioreactors operated continuously are commonly adopted, though batch operation is also possible (Bagatella et al., 2022). Under anaerobic conditions, acidogenic and fermentative bacteria hydrolyze carbohydrates, proteins, and lipids from feedstocks like food waste, cheese whey, or municipal sludge, generating soluble compounds which are further fermented into VFAs such as acetate, propionate, butyrate, and valerate (Bravo-Porras et al., 2024).

The composition and yield of VFAs in the acidogenic reactor depend on feedstock characteristics, operational temperature (mesophilic or thermophilic), HRT, pH (often controlled between 4.5 and 5.5), and OLR, with careful optimization needed to tailor the VFA profile for efficient PHA production and desired copolymer composition, influencing flexibility, melting temperature, and processability (Colombo et al., 2017; Valentino et al., 2015). Importantly, this reactor stabilizes and detoxifies waste streams, reducing solids content and producing a standardized, VFA-rich effluent suitable for subsequent microbial selection and accumulation stages (Albuquerque et al., 2010). Efficient acidogenesis also mitigates the presence of inhibitory compounds such as ammonia or sulfides, promoting overall process robustness and scalability (Bagatella et al., 2022).

By valorizing otherwise problematic organic wastes into customizable VFA blends, the acidogenic reactor underpins sustainable bioplastic production while enabling environmental stewardship and flexible process design (Bravo-Porras et al., 2024; Colombo et al., 2017; Valentino et al., 2015).

1.3.3.2 Selection Reactor

The selection reactor, serves as the pivotal second stage in the three-stage process for PHA production with MMCs, dictating both process efficiency and product quality (Bravo-Porras et al., 2024). Its primary function is to cultivate a microbial community specialized in rapid uptake of VFAs and intracellular PHA storage, even under highly dynamic and non-sterile conditions (Castagnoli et al., 2024). This is achieved by exposing the biomass to alternating

periods of substrate excess (feast) and scarcity (famine) inside SBRs fed with the VFA-rich effluent from the acidogenic stage (Morgan-Sagastume, 2016).

During the feast phase, excess carbon is supplied, prompting the biomass to consume substrate and accumulate PHA, while in the famine phase, the cells must metabolize stored PHA as a carbon source in conjunction with available nitrogen and phosphorus (Bagatella et al., 2022). Over repeated cycles, non-storing microorganisms die off, enriching for PHA-storing bacteria that dominate the SBR community (Morgan-Sagastume, 2016). Key operational parameters include aeration rate, HRT, cycle duration, and OLR are carefully optimized to sustain selection efficacy and stable reactor performance (Castagnoli et al., 2024).

As a result of this regime, the microbial population becomes highly specialized for robust and rapid biopolymer synthesis from diverse VFA feeds, providing system resilience suitable for real waste streams (Bravo-Porras et al., 2024). The adaptable nature of this community ensures consistent PHA production despite fluctuating feedstock qualities, offering a significant advantage over pure cultures prone to contamination and process disruptions. The selection reactor thus underpins the industrial feasibility of MMC-based PHA manufacturing by supporting high yields, flexibility, and circular economy goals (Bagatella et al., 2022).

1.3.3.3 Accumulation Reactor

The accumulation reactor is the final and production-intensive stage of the three-phase process for PHA synthesis using MMCs, where conditions are engineered to maximize intracellular PHA buildup in selected biomass (Bagatella et al., 2022). After transfer from the selection reactor, the specialized microbial consortium is exposed to VFA-rich feed under strict nutrient limitation, usually nitrogen or phosphorus deprivation, which curtails biomass growth and drives metabolic flux toward PHA granule formation at maximum rates (Bravo-Porras et al., 2024).

Key process variables, such as OLR, carbon source profile, temperature, and operational mode (batch, fed-batch, or continuous), are carefully managed to enhance productivity (Colombo et al., 2017). Typically, fed-batch accumulation is controlled online via oxygen monitoring: a spike in oxygen signals carbon depletion, triggering additional feed until oxygen variations stabilize and accumulation concludes (Duque et al., 2014). Under optimal conditions, PHA contents of 40–80% cell dry weight are routinely achieved, rivaling pure-culture systems and enabling the tailoring of PHA copolymer compositions, such as PHBV, for enhanced mechanical and thermal properties (Jin et al., 2023).

A major advantage of this reactor is its ability to efficiently transform heterogeneous, low-value waste into high-density, market-ready biopolymers without sterile conditions (Bagatella et al., 2022). Nevertheless, process control challenges, including substrate fluctuations, VFA inhibition, and microbial dynamic shifts can affect polymer quality and recovery yields, necessitating advanced monitoring. Downstream extraction and purification follows, yielding polymers suitable for industrial and medical applications. Overall, the accumulation reactor is the keystone of waste-derived PHA production, enabling scalable, economical, and sustainable bioplastic manufacturing (Bravo-Porras et al., 2024; Colombo et al., 2017; Duque et al., 2014).

1.3.3.4 Process limitations and hardships

Despite substantial advances in PHA production with MMCs, several key limitations continue to challenge large-scale implementation and consistent process performance. One core difficulty is the variability of both substrate feedstock and microbial community composition, the concentration and makeup of waste-derived VFAs commonly fluctuate due to seasonal and operational factors, resulting in inconsistent polymer yield and monomer composition, and thus unpredictable PHA material properties (Bagatella et al., 2022).

On the biological side, microbial consortia shift in structure and metabolic capability in response to operational or environmental changes, and maintaining the dominance of efficient PHA-storing strains requires carefully managed feast–famine selection (Bedade et al., 2021). The non-sterile nature of MMC processes, while advantageous for cost, increases contamination risks and may require frequent reactor restarts or additional selection to preserve productivity (Bravo-Porras et al., 2024; Morgan-Sagastume, 2016). Operationally, stable performance across acidogenic, selection, and accumulation reactors demands sophisticated real-time monitoring and control over temperature, pH, oxygen, and nutrient levels to avoid suboptimal accumulation or byproduct formation, while harsh and energy-intensive downstream extraction is often needed to obtain polymers of sufficient purity and traceability (Alfano et al., 2021b; Carvalho et al., 2022).

While MMC-based PHA production excels in flexibility, cost reduction, and waste valorization, its limitations, ranging from feedstock heterogeneity and dynamic consortia to challenging process and recovery steps, require ongoing innovation in reactor engineering, monitoring, and community management to realize its full commercial and environmental promise (Colombo et al., 2017).

1.4 Motivation and objectives

Current process configurations for PHA production using MMCs often rely on a dedicated accumulation reactor, which is essential to ensure consistent polymer yield, maintain process stability, and maximize the PHA content within cells. While effective, integrating the accumulation reactor stage adds considerable complexity and cost to the overall process by requiring additional equipment, energy input, and operational oversight. Furthermore, the division between biomass enrichment and PHA accumulation phases, while frequently practiced, extends the processing time and increases waste generation. Therefore, in this work the aim is to simplify and streamline the PHA production process by targeting a reduction or complete removal of the accumulation reactor. Achieving this would result in a more efficient, compact system with reduced capital and operational expenses, enhancing the economic attractiveness and scalability of PHA production with MMC.

One promising approach is to operate a SBR under dynamic feast–famine (F/F) conditions as selective pressure, adjusting the biomass purge to occur after the feast phase instead of the end of the famine phase. This adjustment is driven by the hypothesis that the timing of biomass withdrawal strongly influences the selection and retention of PHA-rich microbial populations like the traditional purge after the famine phase, thus potentially increasing the average polymer content of the harvested biomass even in the absence of a separate accumulation . R. A. P. Cruz et al. (2022) attempted this strategy but they observed a decrease in global PHA productivity due to losses in biomass productivity, this is probably a result of the reduction in N&P solution fed as they adjusted the volume considering the 1/8 purged from the SBR. In this present study, this strategy will be attempted feeding the N&P solution without said adjustment to try to increase the biomass productivity, and, as a consequence, the overall PHA productivity. It is expected that the accumulation phase will be faster and need less carbon pulses as a result of purging biomass from the SBR with more PHA.

To further exploit the potential of a SBR configuration, the operational strategy is extended by changing the feeding strategy to increase the OLR through the addition of two carbon pulses during the feast period in each cycle. This strategy was adopted so the OLR could increase without risking inhibition by substrate. As Matos et al. (2021a) observed, above the 5.4 g-COD/(L·d) there was a decrease in PHA yield in relation to VFAs fed and an increase in F/F ratio. However, this study attempted to feed the fermentation products (FPs) in one carbon pulse instead of dividing them into two smaller pulses, thus avoiding inhibition by substrate. Importantly, this is performed without a concomitant increase in nitrogen and phosphorus

supplementation, relying on the natural metabolic regulation of nutrient-limited cells to promote PHA synthesis over biomass growth. If successful, this dual-pulse strategy, combined with post-feast biomass withdrawal, could enhance PHA accumulation within the main reactor, reducing or even eliminating the necessity for an external accumulation reactor, and yield a process that is both more stable and resource-efficient. This study will therefore evaluate whether reactor stability can be maintained under these intensified conditions and whether significant improvements in PHA content can be achieved, making a compelling case for process simplification in industrial PHA production. Besides the points mentioned above, this study will also evaluate the physical and mechanical properties of the polymers produced in each condition to better understand and measure how the change in methodology can impact the final PHA, considering that it is very important to improve the production without compromising the final quality of the polymer.

2

MATERIALS AND METHODS

2.1 PHA Production

A tree-stage methodology was adopted to produce PHA (**Figure 2.1**). In the first stage, apple pulp waste was fed to a UASB reactor that converted the sugars into VFAs subsequently used to feed a SBR inoculated with sludge from a wastewater treatment plant. In the SBR, the FPs were converted into PHA and a PHA-accumulating MMC culture was selected. In the last stage, the MMC purges collected from the SBR were used in a fed-batch bioreactor operated to maximize PHA accumulation by feeding pulses of FPs from the UASB reactor. The current work focused on the operation of the SBR and accumulation bioreactors.

The apple pulp waste, supplied by Sumol+Compal S.A., was the feed used for the UASB reactor.

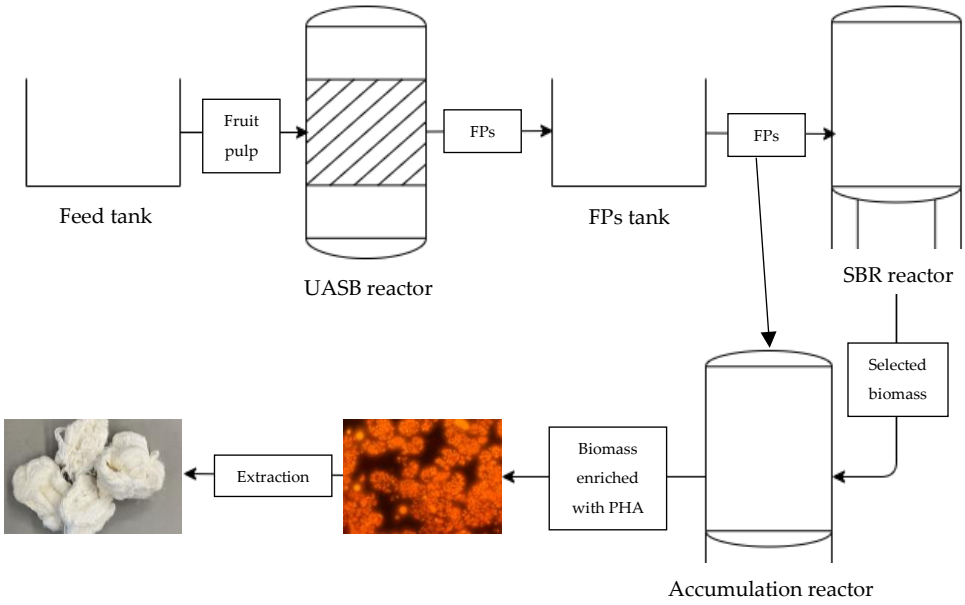

Figure 2.1-Simplified scheme of the three-stage process for PHA production.

2.1.1 Sequencing-batch reactor (SBR)

The SBR was used to select PHA producing bacteria from activated sludge with a feast and famine strategy as selective pressure. In this study, three different operating conditions were investigated: (**1**) Biomass purge in the famine, the traditional mode of operation, with one carbon pulse; (**2**) Purge at the end of the feast, keeping the same carbon amount and (**3**) Purge at the end of the feast with two carbon pulses. The strategy of purging biomass with higher PHA content at the end of the feast (Operation 2) proposed in this study intended to assess if the higher PHA content within the biomass purged could reduce the time and/or cost associated with the accumulation process. To further reduce, or even eliminate, the need for the PHA accumulation step, another strategy was studied (Operation 3), during which the purge was kept at the end of the feast, but two carbon pulses were fed to the reactor in order to increase the PHA content of the biomass inside the SBR.

2.1.1.1 Feedstock

The UASB operation was performed with a recirculation flow rate within the range of 0.88 to 1.00 L/min, internal pressure between 0.0-0.2 Pa, pH controlled at 4.80-4.90, 30 °C and an HRT of 1 day. The OLR was set to 5 g-COD/(L·d) during the first days of operation, which was gradually increased over time up to 25 g-COD/(L·d). The reactor was operated over 10 months and was used to produce a VFA rich stream needed for the SBR and accumulation reactor, it was not monitored in the context of the current work.

The FPs used as feedstock averaged a composition of 0.03 ± 0.00% g-COD of lactate, 7.66 ± 0.02% g-COD of acetate, 4.52 ± 0.02% g-COD of propionate, 0.32 ± 0.00% g-COD of ethanol, 0.32 ± 0,00% g-COD of isobutyrate, 72.90 ± 0.01% g-COD of butyrate, 12.38 ± 0.02% g-COD of valerate and 2.06 ± 0.03% g-COD of caproate (**Figure 2.2**). HB and HV precursor ratio were 83.10:16.90 (%g-COD:%g-COD).

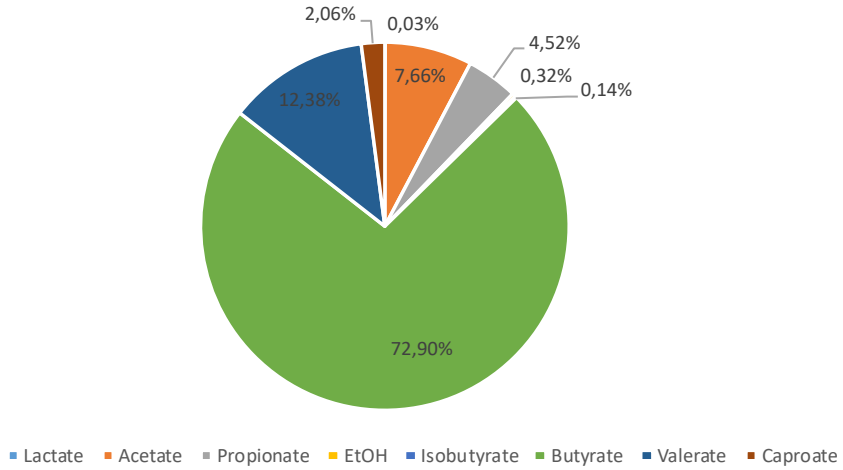

Figure 2.2-VFAs and ethanol ratio in the FPs (%g-COD).

2.1.1.2 Operation

The SBR was inoculated with activated sludge from a wastewater treatment plant (Mutela, Almada, Portugal). This bioreactor of 150 L was operated with an HRT of 1 day and a sludge retention time (SRT) of 4 days in 12 h cycles, pH of 7.5-8.5, temperature between 17-20 °C, air flow rate and stirring set to keep the oxygen saturation inside the reactor above 20%. Dissolved oxygen (DO) and pH were continuously measured. When inoculated, the initial OLR was 3 g-COD/(L·d) and after the culture stabilizes, it was increased to 5.5 g-COD/(L·d) as Matos et al. (2021) described the optimum OLR at 5.4 g-COD/(L·d).

The cycle begins with the feast phase where a mineral solution, described in Serafim et al. (2008) with minor modifications (dipotassium phosphate and monopotassium phosphate were not used), and the fermented feedstock were added to the reactor, for 15 minutes. After 2 hours of the beginning of the cycle, an ammonium chloride (NH_4Cl) (ITW Reagents, Italy) and potassium di-hydrogen phosphate (KH_2PO_4) (ITW Reagents, Italy) solution was added to the reactor at a C:N:P molar ratio of 100:7:1 (C-mmol:Nmmol:P-mmol). In a cycle, the aerated feast and famine were about 45 min and 10 h, respectively, 15 min were for biomass purging either after feast or famine depending on the operation, the last 1 h of the cycle was for biomass settling and supernatant withdrawal to restore the volume for the beginning of the next cycle.

Briefly, the reactor's operation with purge in the famine (Operation 1) was performed at an OLR of 5.5 g-COD/(L·d) and the purge was set to the end of the famine phase, right before the settling and withdrawal. This is the traditional method for operating this reactor. Between Operation 1 and 2 the reactor was reinoculated. Then, the timing of the purge was changed to 90 minutes after the beginning of the feast phase (Operation 2) to assure the feast was over and the N&P solution was not fed before purging. Lastly, Operation 3, the reactor was fed with two carbon pulses, each one corresponding to what was given at 5.5 g-COD/(L·d), spaced

30 minutes between them, totaling 11 g-COD/(L·d) and the biomass was purged after the feast phase like in Operation 2. To increase the PHA content of the biomass and avoid excessive biomass volumetric productivity over the cycles, the volume of N&P solution fed was kept the same as the previous operations, which theoretically cuts the C:N ratio (C-mmol:N-mmol) in half. A summary of the differences between Operations 1,2 and 3 can be found in **Table 2.1**.

Table 2.1-Summary of the main differences between Operations 1, 2 and 3.

Parameter	Operation 1	Operation 2	Operation 3
Inoculum	Activated sludge	Activated sludge	Biomass from Operation 2
Days of operation (d)	81	82	40
OLR (g-COD/(L·d))	5.5	5.5	11
Number of carbon pulses	1	1	2
C:N:P (C-mmol:N-mmol:P-mmol)	100:7:1	100:7:1	100:3.5:1
Purge Timing	End of famine	End of feast	End of feast

All operating parameters (except OLR in Operation 3) and volume of solutions added were maintained all throughout. After three stable SRTs (12 days) with no changes in the F/F ratio, three SBR cycle monitorings were performed for each operation, samples were collected along the cycle for FPs, PHA, NH_4^+, total suspended solids (TSS) and volatile suspended solids (VSS) quantification. During the feast, 5 samples per carbon pulse were taken, 5 samples were taken during the carbon consumption and 3 during the consumption of the N&P solution, for Operations 2 and 3 one sample was taken before and one after the purge.

2.1.2 PHA accumulation

In order to maximize PHA production, fed-batch accumulation assays were carried out in a 60 L reactor, inoculated with biomass from the selection SBR during Operations 1, 2 and 3, and fed with pulses of FPs controlled by DO. The accumulation was carried out until the previous pulse stopped having an abrupt increase in DO at the end of the fermented consumption and there was no oxygen decrease to FPs, it was ended by adding sulfuric acid (Honeywell Fluka™, USA) until pH 2 and the biomass was stored at 4 °C till extraction. These assays were performed at 18-23 °C with aeration and stirring set to keep oxygen saturation above 20%. pH and DO were monitored using online sensors, and a hydrochloric acid (HCl) (ITW Reagents, Italy) 5M solution was used to control the pH setpoint at 8.5.

Samples were taken throughout the assays for FPs, PHA and TSS/VSS analysis, at the beginning, middle and end of each pulse.

The operating parameters were maintained for all operations to ensure that no changes could be attributed to different methods used during the accumulations.

2.2 Analytical Procedures

The samples taken from the selection SBR and from the PHA accumulation bioreactor were centrifuged (13500 rpm/12300 g for 2 min), the supernatant was filtrated using a 0.2 μm membrane filters, the pellet was frozen at -20 °C and posteriorly lyophilized. For TSS/VSS the samples were directly without centrifuge.

2.2.1 FPs quantification

FPs were measured in filtered samples (0.2 μm) through HPLC in a Merck-Hitachi chromatographer with an Aminex HPX–87H pre-column and column coupled to an infrared (IR) and a diode array detector (DAD). The following conditions were used: column temperature 30 °C, 0.01 N H_2SO_4 eluent, flow rate 0.5 mL/min and injection volume 99 μL. The FP concentrations were calculated using standard calibration curves from 4 – 1000 mg/L of lactate (Sigma-Aldrich, Germany), acetate (Fisher scientific, USA), propionate (Sigma-Aldrich, Germany), isobutyrate (Sigma-Aldrich, Germany), ethanol (Carlo Erba, Italy), butyrate (PanReac AppliChem, Germany), valerate (Thermo Scientific, USA), and caproate (Thermo Scientific, USA).

2.2.2 Nitrogen quantification

Soluble ammonia (NH_4^+) concentration was assessed in filtered samples (0.2 μm) using a colorimetric method implemented in a segmented continuous flow analyzer (Skalar SNA++, Skalar Analytical, Netherlands).

2.2.3 TSS&VSS analysis

Total suspended solids (TSS) and volatile suspended solids (VSS) were determined according to standard methods (Clesceri et al., 1999).

2.2.4 Qualitative PHA Detection

Nile Blue staining was used as a qualitative technique to evaluate the presence of PHA in the microbial culture. To 1.5 mL of biomass sample from the end of the feast phase of the SBR, 5 μL of a 0.2% aqueous solution of Nile Blue (Sigma-Aldrich, Germany) was added and incubated at 100 °C for 10 minutes. The sample was then observed in a microscope (Carl Zeiss Microscopy GmbH, Germany) under fluorescent light (Carl Zeiss Microscopy GmbH, Germany).

2.2.5 PHA quantification and composition

Intracellular PHA content and monomeric composition were determined using gas chromatography (GC). In a tube, lyophilised biomass samples (1.5-5 mg) were treated with 1 mL of an acidic methanol (Fisher Chemical, USA) solution (acidified with sulfuric acid 20% (v/v) (Honeywell Fluka™, USA)) mixed with 1 mL of a chloroform (Honeywell Riedel-de Haën™, USA) with 0.5 g/L of heptadecane (Sigma-Aldrich, USA). This mixture was heated in sealed glass tubes at 100 °C for 3.5 hours to ensure complete methanolysis. After the tubes cooled down, 1 mL of water was added and mixed in the vortex for 30 seconds, and the tubes were then left for 1 hour to ensure maximum phase separation. The water phase was removed, and 1 mL of water was added again to repeat the washing process. Afterwards, the organic phase was extracted into a GC vial with molecular sieves for water removal and then filtered with 0.2 μm PTFE filters (LABFIL, China) to a new vial to be encapsulated. The standards used for this analysis were 3-hydroxybutyric acid (3-hydroxybutyrate, HB) (97%, Thermo Scientific, USA), 3-hydroxyvaleric acid (3-hydroxyvalerate, HV) (98%, Med-ChemExpress, USA) and methyl-3-hydroxyhexanoic acid (3-hydroxyhexanoate, HHx) (97%, Sigma-Aldrich, USA) with concentrations between 0.05 and 1.0 g/L. After sample preparation, 1.0 μL was injected into a gas chromatographer, equipped with a flame ionization detector (FID) (TRACE 1300, Thermo Scientific, USA) and a column of 60 m, 0.53 mm ID, 1 μM df, Crossbond, Stabilwax (Restek, USA). The analysis was conducted using helium as the carrier gas at a constant pressure of 14.5 psi. The injection temperature was set to 280 °C, the detector temperature to 230 °C, and the temperature ramp started at 40 °C. The temperature increased at a rate of 20 °C/min until reaching 100 °C, then increased at a rate of 3 °C/min until reaching 175 °C and finally increased at a rate of 20 °C/min until reaching 220 °C to ensure proper cleaning of the column after each injection.

2.2.6 PHA Extraction and Purification

The PHA-enriched acidified biomass obtained from the accumulation assays was centrifuged, supernatant discarded and freeze-dried (Scanvac CoolSafe 110-4, Labogene) to ensure complete water removal. The dried biomass was then weighed and suspended in chloroform (Honeywell Riedel-de Haën™, USA) at a ratio of 5 mL of solvent per gram of dry biomass. The mixture was incubated at 60 °C under constant agitation (250 rpm) for 5 hours. Following this process, the suspension was maintained at 30 °C until the next step. Undissolved materials were removed using a paper filter via vacuum filtration, and the resulting filtrate was left in a fume hood until the solvent had completely evaporated. The obtained crude polymer was then weighed.

For purification, the crude polymer was redissolved in chloroform (Honeywell Riedel-de Haën™, USA) and precipitated in ice-cold ethanol (1:10% v/v) under vigorous stirring. The precipitated polymer was collected and allowed to dry at room temperature inside the fume hood. To ensure the complete removal of ethanol, an additional drying step was performed in an oven at 35 °C. The purified polymer was subsequently weighed and stored in the dark for further analysis.

2.2.7 PHA characterization

2.2.7.1 Thermo-gravimetric Analysis (TGA)

TGA (Labsys EVO Analyser, Seteram) was used to determine the degradation temperature (T_{deg}) of the polymers, it was considered the point in the TG curve where the sample had 5% mass loss. For this, 10 mg of each pure polymer was weighed and analysed between room temperature and 500 °C, at a rate of 10 °C/min and with a weighing precision of ± 0.01%, under an argon atmosphere.

2.2.7.2 Molecular weight

Number and average molecular weights, M_n and M_w, respectively, and the dispersity ($Đ_M = M_w/M_n$) of the PHA samples were determined by a gel permeation and size exclusion chromatography (GPC/SEC) System (KNAUER Smartline, Germany), using a Phenomenex Phenogel Linear Liquid Chromatographic Column 300×7.8 mm (Phenomenex, USA) coupled with the refractive index detector (RID) Waters2414 (Waters, USA). The samples were dissolved in

chloroform (concentration range: 0.3 – 0.4%, w/v) and monodisperse polystyrene standards (370 – 2520,000 Da) were used.

The solutions were injected (100 µL) and the analysis was performed at 30 °C, with a flow rate of 1 mL/min of chloroform as mobile phase.

2.2.7.3 Differential Scanning Calorimetry (DSC)

DSC using a TA DSC-Q2000 instrument was employed to analyze the thermal properties of the extracted polymers. Approximately 5 ± 0.5 mg of each sample, prepared in duplicate, were weighed and sealed in aluminum crucibles. All measurements were conducted under a nitrogen atmosphere (50 mL/min).

Initially, a thermal pre-treatment was carried out to eliminate any prior thermal history. The samples were heated from 20 °C to 180 °C at a rate of 10 °C/min and held isothermally for 1 minute to ensure complete melting of the polymers. To prevent immediate crystallization, they were then rapidly cooled to room temperature at 50 °C/min and stored in a desiccator for at least 14 days, allowing slow crystallization to occur.

After the aging period, the samples underwent a second heating from room temperature to 180 °C at 10 °C/min, followed by a 3-minute isothermal hold. They were then cooled to −70 °C at 10 °C/min, held isothermally for 5 minutes, and subjected to subsequent heating cycles. The second and third heating ramps were identical to the first, while the second cooling ramp—after the second heating—was performed at approximately 50 °C/min.

The first heating cycle was used to determine the melting point (T_m) and melting enthalpy (Δ_m). The first cooling ramp provided data for the melt crystallization temperature (T_c), while the final heating ramp was used to determine the glass transition temperature (T_g) and cold crystallization temperature (T_{cc}).

2.2.7.4 Mechanical properties

The mechanical properties of the PHA samples were evaluated through uniaxial tensile testing. Test specimens were fabricated by dissolving 2 g of purified polymer in 20 mL of chloroform and, using a casting knife, a film with a thickness of 150 µm was made. Samples were then cut with a width of 1.5 cm and a length of 5 cm, the thickness was verified with a caliper to ensure consistency and accurate calculations of engineering stress and strain.

Tensile experiments were carried out using a food texture analyzer (TMS-Pro, Mecmesin and Food Technology Corporation, United Kingdom) equipped with a 250 N load cell and a

clip-on extensometer for accurate strain measurement. The tests were performed at a constant crosshead speed of 10 mm/min. Each sample was loaded progressively until rupture.

Stress was determined as the applied force divided by the initial cross-sectional area of the specimen, while strain was obtained as the ratio of extension to the original gauge length. Stress–strain curves were plotted for each test. From these curves, Young's modulus was calculated from the slope of the initial linear elastic region, the ultimate tensile strength (UTS) was defined as the peak stress before specimen failure, and the elongation at break was recorded at the point of fracture. All experiments were conducted in ambient laboratory conditions, with at least five replicates performed to ensure reproducibility and statistical reliability of the results.

2.3 Calculations

The feast-to-famine ratio (F/F ratio, h/h) was determined by dividing the duration of the feast phase by that of the famine phase. PHA content within the biomass (% w/w) was quantified by calculating the proportion of PHA to the VSS measured concurrently during the experiment. The concentration of active biomass (X_a, g-X_a/L) was obtained by subtracting the amount of PHA (g/L) from the VSS concentration (g/L) at each reaction time point.

Biomass volumetric productivity (XPR, g-X_a/(L·d)) was derived by dividing the active biomass concentration (g-X_a/L) by the SRT (d). Specific rates, including substrate uptake (-q_{FP}, g-COD_{FP}/(g-COD_{Xa}·d)), PHA accumulation (q_{PHA}, g-COD_{PHA}/(g-COD_{Xa}·d)), and PHA consumption during famine (-qPHA famine, g-COD_{PHA}/(g-COD_{Xa}·d)), as well as the maximum specific growth rate (q_{Xa}, h^{-1}), were estimated from the slopes of the linear phase of the linear regressions for total FP, PHA, and X_a concentrations over time. PHA productivity in the accumulations (rPHA, g-PHA/(L·d)) was calculated by dividing the difference in PHA (g-PHA/L) until maximum PHA value by the time it took to reach it (h). The quality of these regressions was verified with R^2 values greater than 0.85.

PHA yield (g-COD_{PHA}/g-COD_{FP}) was assessed by dividing qPHA by -qFP. The growth yield in famine ($Y_{X/PHA}$, g-COD_{Xa}/g-COD_{PHA}) was determined by dividing the amount of active biomass generated by the total PHA consumed.

Global PHA productivity (g-PHA/(L·d)) was calculated multiplying the biomass volumetric productivity (g-X_a/(L·d)) in the SBR by the maximum PHA accumulated during the accumulation (g-PHA/L), and then dividing by the active biomass inoculated in the accumulation (g-X_a/L).

Global PHA yield (g-COD_{PHA}/g-COD_{FP}) was determined dividing the kg-COD_{PHA} (kg-COD correspondent to 1 kg of PHA) by the total kg-COD_{FP} needed to produce 1 kg of PHA. The total kg-COD_{FP} includes both the COD from the feeding substrate consumed during accumulations and the COD used to produce the necessary biomass to generate 1 kg of PHA.

All g-COD results come from the conversion of g to g-COD using the oxidation stoichiometric conversion ratios of 1.06 g-COD/g-lactate, 1.06 g-COD/g-acetate, 1.51 g-COD/g-propionate, 2.08 g-COD/g-ethanol, 1.81 g-COD/g-isobutyrate, 1.81 g-COD/g-butyrate, 2.04 g-COD/g-valerate, 2.21 g-COD/g-caproate, 1.67 g-COD/g-HB, 1.92 g-COD/g-HV and 1.41 g-COD/g-X_a (considering the chemical formula of $C_5H_7NO_2$ defined by (Gujer & Henze, 1991)).

3
RESULTS AND DISCUSSION

3.1 Sequencing Batch Reactor

In Operation 1, the reactor was operated with an OLR of 5.5 g-COD/(L·d) and the purge was set to end of the famine phase, before settling and withdrawal steps. The SBR started with an OLR of 3 g-COD/(L·d). After 10 cycles (5 days) the F/F ratio decreased from 0.17 to 0.08 as can be observed in **Figure 3.1** and the OLR was increased to 5.5 g-COD/(L·d). After increasing the OLR, the F/F ratio stabilized again at cycle 38 (19 days after inoculation), averaging 0.03 ± 0.01 until the end of the reactor's Operation 1 at cycle 165 (day 81) (**Figure 3.1**), under the established value of 0.3 as the maximum reference commonly used (Reis et al., 2011). This F/F ratio falls in line with what is observed in other studies working with similar OLR, SRT, HRT and feedstock (Matos et al., 2021a, 2021b). The decline of the F/F ratio in the early stages of each OLR indicates that a selection pressure is being exerted and the number of PHA-accumulating bacteria is increasing (Duque et al., 2014).

In **Figure 3.2 A** is represented an example of one cycle monitoring for this operation, as can be observed, at the onset of the feeding period, a decline in the FPs' concentration was observed, indicating that the prevailing organic acids were being consumed (**Figure 3.2 A**). These acids were subsequently converted into PHA, as evidenced by an escalation in the intracellular PHA content, reaching a peak at the culmination of the feast phase, **Figure 3.3** shows the culture observed in the microscope and PHA granules can be observed. Following the consumption of the FPs, a transition to a state of food scarcity is triggered and, with the addition of the N&P solution at 2.20 h of the cycle, prompts the utilization of PHA by accumulating microorganisms for growth (**Figure 3.2 A**). After the feeding and consumption of the nitrogen available, the active X_a growth stabilizes, with PHA consumption serving solely for cellular maintenance and survival. At the end of the famine phase for Operation 1, the reactor is purged and the biomass goes to the accumulation reactor to increase the intracellular PHA content (**Figure 3.2 A**).

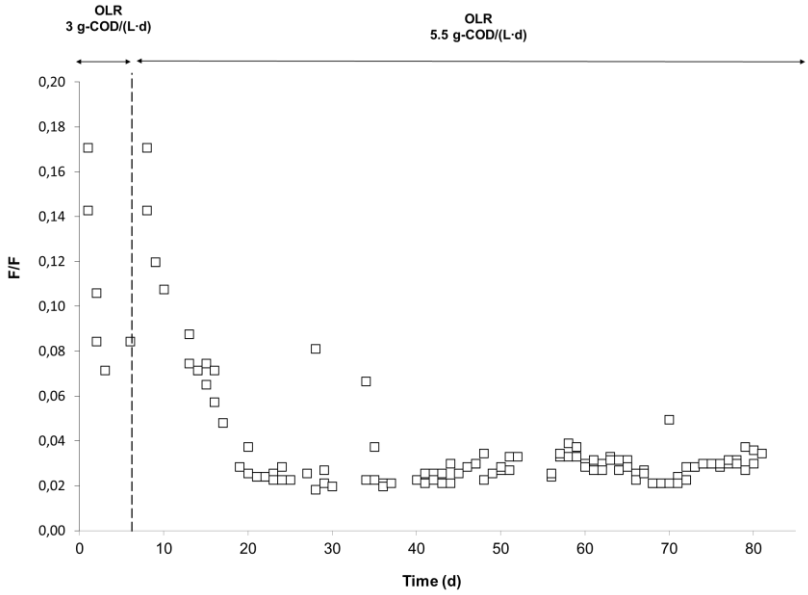

Figure 3.1-F/F ratio (h/h) profile of the SBR cycles during Operation 1.

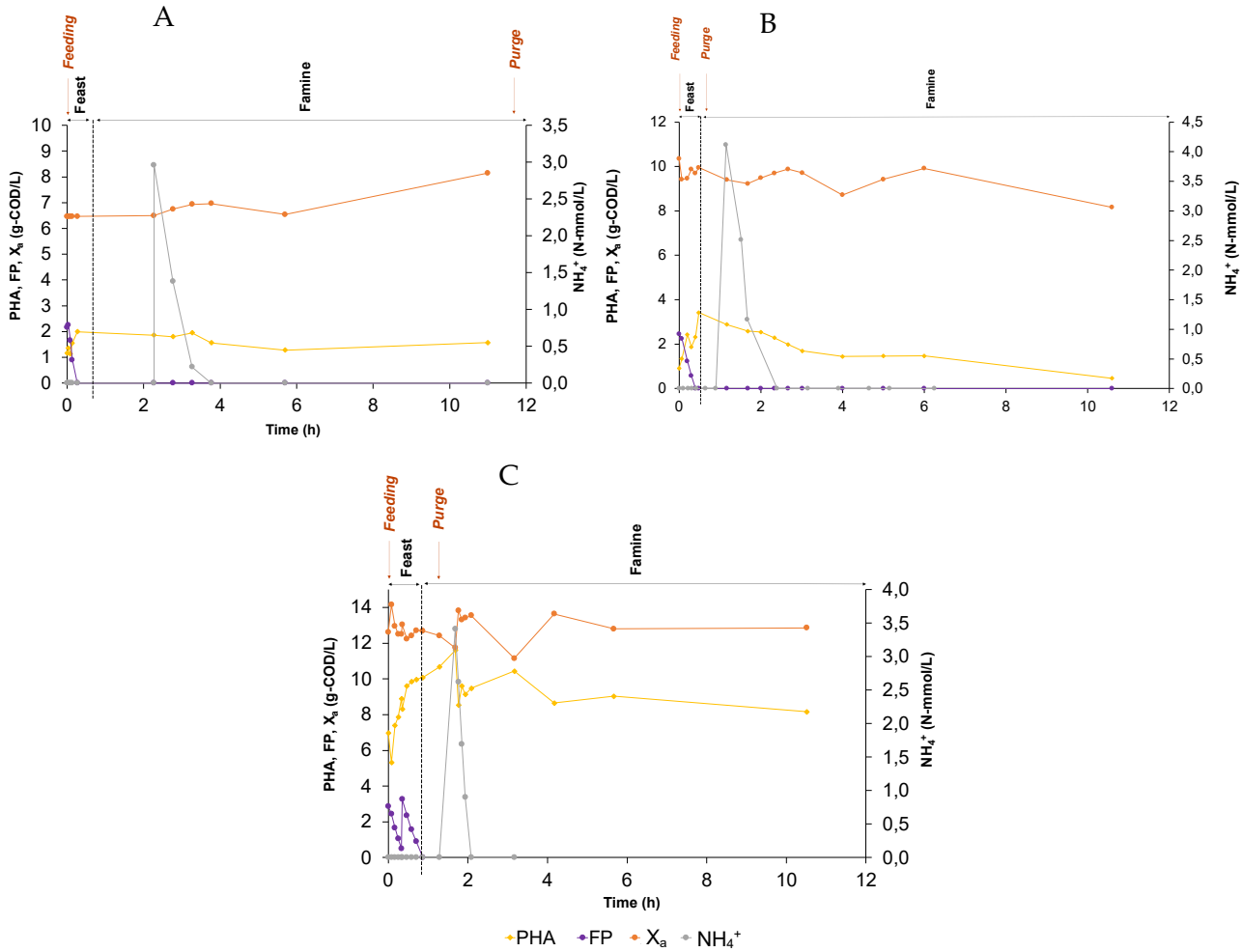

Figure 3.2-Typical profile of an SBR cycle during Operations 1 (A), 2 (B) and 3 (C) with its respective PHA (g-COD/L), FP (g-COD/L), X_a (g-COD/L) and NH_4^+ (N-mmol/L) contents during the first 6 hours of the cycle.

The results obtained in Operation 1 (**Table 1**) demonstrate the effectiveness of the traditional operation method to select PHA-accumulating bacteria. The maximum PHA content was 21 ± 3% (g-PHA/g-TSS) at the end of the feast and a minimum PHA content at the end of the cycle of 11.8 ± 0.1% (g-PHA/g-TSS), achieving a PHA yield of 0.66 ± 0.02 g-COD_{PHA}/g-COD_{FP} and 0.9 ± 0.3 g-PHA/L (**Table 1**). The volumetric productivity of X_a was 1.3 ± 0.1 g-X_a/(L·d) (**Table 1**). Rangel et al. (2023) showed similar results with an F/F ratio was closely the same at 0.09 and the VSS were higher at 7.0 g-VSS/L, the higher X_a at 6.5 g-X_a/L is due to the slightly higher OLR that requires the addition of more nitrogen, which are the conditions needed for higher active biomass. In terms of PHA yield, they observed a maximum PHA content during the feast of 17.7 ± 1.9% (g-PHA/g-TSS) despite the slight difference in OLR (theirs was 150 Cmmol/(L·d), ours was 137 ± 37 Cmmol/(L·d)) and using a feedstock composed mainly of acetic, lactic and butyric acids, and ethanol resultant from the acidogenic fermentation of effluent from the confectionery industry. They also employed the traditional method with the purge at the end of the famine phase, an SRT of 4 days and an HRT of 1 day. Their overall results for the SBR were similar to ones in this study.

Matos et al. (2021b), in a study to evaluate the impact of the SRT on the SBR, used a three-stage process for PHA production from fruit pulp waste, the experimental setup was slightly different as their SBR had a volume of 100 L. An HRT of 1 day, an SRT of 4 days and an OLR of 5.4 g-COD/(L·d) were used. The results achieved resembled our work, achieving an active biomass of 4.84 ± 0.02 g-X_a/L despite having a higher PHA yield of 0.90 ± 0.04 g-COD_{PHA}/g-COD_{FP} compared to the one obtained in this study of 0.66 ± 0.02 g-COD_{PHA}/g-COD_{FP}. Their $q_{PHAfeast}$ was lower at 0.93 ± 0.03 g-COD_{PHA}/(g-COD_{Xa}·h), but the ΔPHA during the feast was double ours at 18.2 ± 0.3% (g-PHA/g-TSS). These differences can be attributed to the volume of their SBR as a smaller volume might facilitate carbon and oxygen transfer, resulting in a different MMC selected, as they mention having up to 93% of PHA-accumulating bacteria. The results obtained for the operation with the purge after the famine phase (Operation 1) align with studies using similar experimental setups and parameters, and will be used as a benchmark for comparison with the other strategies testes in this study.

After Operation 1, the SBR was reinoculated for Operations 2 and 3, where the purge after feast and the OLR of 11 g-COD/(L·d) with purge after the feast were tested, respectively. The SBR demonstrated a period of eight days to reach a consistent F/F ratio under 0.06 at an OLR of 3 g-COD/(L·d), similar to what happened in Operation 1. Subsequently, the OLR was elevated to 5.5 g-COD/(L·d). Following the monitoring of SBR's Operation 2 on days 71 and

72, the OLR was augmented to 11 g-COD/(L·d) (**Figure 3.4**) for Operation 3 and remained like this until the end of the experimental period. The monitoring for Operation 3 was performed on days 121 and 122 since reinoculation.

Table 3.1-Summary of the controlled parameters during the SBR monitoring for Operations 1,2 and 3. Data was displayed as Average SD (n=2).

Parameter	Operation 1	Operation 2	Operation 3
OLR (g-COD/(L·d))	5 ± 2	5.1 ± 0.2	10.9 ± 0.4
OLR (Cmmol/(L·d))	137 ± 37	129 ± 56	274 ± 11
F/F ratio (h/h)	0.024 ± 0.002	0.033 ± 0.002	0.079 ± 0.001
VSS (g-VSS/L)	6.1 ± 0.5	7.7 ± 0.8	14.2 ± 0.7
XPR (g-X_a/(L·d))	1.3 ± 0.1	1.66 ± 0.02	2.09 ± 0.04
X_a (g-X_a/L)	5.1 ± 0.5	6.64 ± 0.08	8.4 ± 0.2
(-) q_{FP} (g-COD_{FP}/(g-COD_{Xa}·h))	1.50 ± 0.03	0.93 ± 0.05	0.54 ± 0.04
Average PHA during feast (% (g-PHA/g-TSS))	15 ± 4	13 ± 5	32 ± 4
Minimum PHA in feast (% (g-PHA/g-TSS))	11.8 ± 0.1	5.6 ± 0.9	27 ± 1
Maximum PHA in feast (% (g-PHA/g-TSS))	21 ± 3	19.9 ± 0.5	40.4 ± 0.2
PHA in purged biomass (% (g-PHA/g-TSS))	11.25 ± 1.76	19.9 ± 0.5	40.4 ± 0.2
$q_{PHA\ feast}$ (g-COD_{PHA}/(g-COD_{Xa}·h))	1.3 ± 0.2	0.7 ± 0.1	0.52 ± 0.06
(-) $q_{PHA\ famine}$ (g-COD_{PHA}/(g-COD_{Xa}·h))	0.03 ± 0.01	0.09 ± 0.01	0.45 ± 0.04
PHA Yield (g-COD_{PHA}/g-COD_{FP})	0.66 ± 0.02	0.80 ± 0.08	0.96 ± 0.03
q_{Xa} | famine (h^{-1})	0.03 ± 0.01	0.08 ± 0.01	0.37 ± 0.09
$Y_{Xa/PHA}$ (g-COD_{Xa}/g-COD_{PHA})	0.58 ± 0.02	0.742 ± 0.003	0.828 ± 0.001

During Operation 2, significant alterations were expected in the SBR since R. A. P. Cruz et al. (2022) noted, more importantly, an increase in PHA content and a decrease in biomass from the traditional operation to the one purging after the feast like in the present study. As can be observed in **Figure 3.4**, the F/F ratio remained consistent under 0.06 during Operation 2,

indicating that the selection pressure remained unaltered and good. As the OLR was kept at 5.5 g-COD/(L·d) in both Operations 1 and 2, the maximum PHA content remained unaltered by the change in purge timing (21 ± 3% (g-PHA/g-TSS) in Operation 1 and 19.9 ± 0.5% (g-PHA/g-TSS) in Operation 2) (**Table 3.1**). The cycle's profile looks similar to Operation 1, with the main difference being the time of the purge and the increase in X_a (**Figure 3.2 B**).

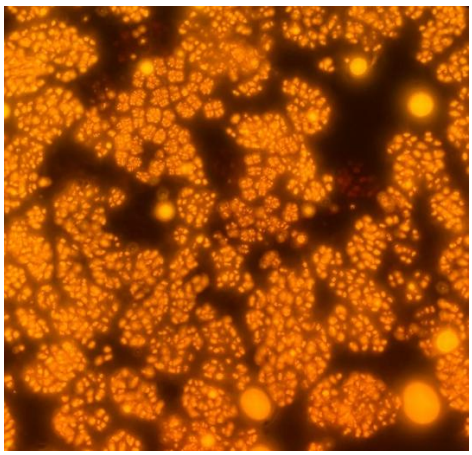

Figure 3.3-SBR's MMC observed with Nile blue staining in the microscope.

As expected, the $Y_{Xa/PHA\ famine}$ was higher (0.58 ± 0.02 g-COD_{Xa}/g-COD_{PHA} in Operation 1 and 0.742 ± 0.003 g-COD_{Xa}/g-COD_{PHA} in Operation 2), meaning that more PHA is being consumed during the famine for biomass growth, reflected in the minimum and maximum values of PHA content during the feast, which will cause an increase in active biomass (5.1 ± 0.5 g-X_a/L in Operation 1 and 6.64 ± 0.08 g-X_a/L in Operation 2). A notable increase was observed in biomass volumetric productivity, with values of 1.3 ± 0.1 g-X_a/(L·d) in Operation 1 and 1.66 ± 0.02 g-X_a/(L·d) in Operation 2. Both biomass volumetric productivity and active biomass increases in relation to the benchmark operation can be explained by maintaining the N&P solution's volume. R. A. P. Cruz et al. (2022) attempted a three-stage process involving purging at the end of the feast. However, in their study, the amount of nitrogen was calculated based on the carbon remaining after biomass purging, rather than the carbon fed in Cmmol. In practical terms, they assume that if they purge 1/8 of the reactor before adding the N&P solution, then the volume of N&P solution fed to the reactor has to decrease 1/8. Meanwhile, in the present study, this adjustment was not made, and we considered the ratio to be based on the amount of carbon fed to the reactor during the feeding. This difference in methodology is enough to contribute to the bigger biomass growth and lower maximum PHA content observed in the present study. Furthermore, R. A. P. Cruz et al. (2022) noted a tripling in the F/F ratio, almost a double in the maximum PHA content during the feast and a fourth in biomass volumetric

productivity when compared to the control reactor operated with the purge at the end of the famine phase. The effects observed in the aforementioned study resemble a butterfly effect as the simple reduction in the volume of N&P solution led to a decrease in active biomass, which subsequently reduced biomass productivity. Moreover, since the same amount of carbon was supplied to a smaller biomass concentration, the F/M ratio (Food/Microorganism) increased in favor of PHA accumulation, as the carbon load was too high for the capacity of the biomass inside the SBR. In a way, it worked as Operation 3 of the present study intended, since there was an increase in PHA content inside the SBR but with the side effect of losing biomass productivity.

In summary, the primary benefit of purging biomass after the end of the feast phase in Operation 2 is the higher PHA content and increased biomass volumetric productivity. At the time of the purge, a higher PHA content is observed which can possibly result in a reduced number of pulses during the accumulation phase, leading to a decreased duration and complexity of the overall process and a decrease of the total carbon needed to achieve the same PHA production.

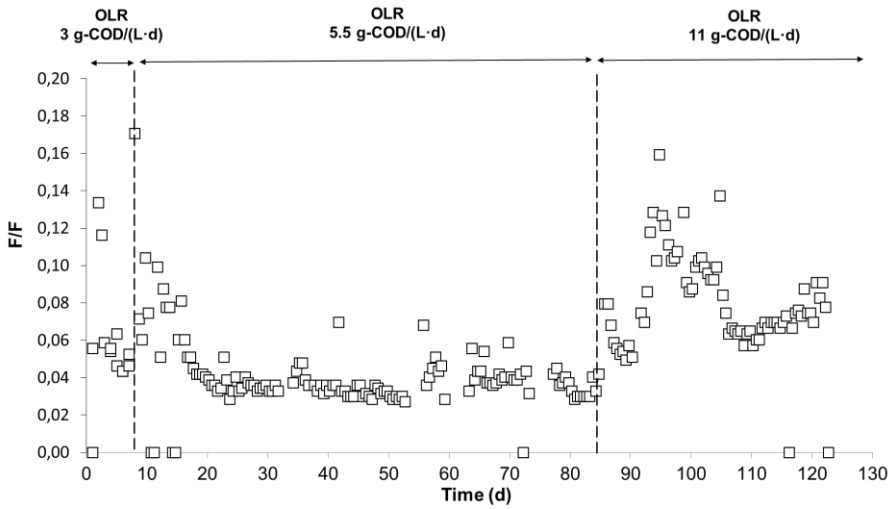

Figure 3.4-F/F ratio (h/h) profile of the SBR cycles during Operations 2 and 3.

In Operation 3, a two-pulse feeding strategy was adopted, as a way to increase the OLR of the reactor without provoking inhibition. According to the Michaelis-Menten equation, the reaction rate within a reactor varies with substrate concentration. For our operating conditions, Matos et al. (2021a) define the concentration as an OLR of 5.4 g-COD/(L·d). At 11 g-COD/(L·d), Matos et al. (2021a) states that inhibition by substrate should exist and by trying to keep the concentration optimum, the possibility for OLR and PHA content increase is created. This designed pulse-feeding strategy mimics the feeding method used in accumulations.

Since the N&P solution added was not proportionally increased to the double, the biomass growth was not stimulated in the same proportion. As the F/M ratio doubled, the F/F ratio was expected to also increase in comparison to Operations 1 and 2, preposition that was confirmed with an F/F ratio of 0.079 ± 0.001 (**Table 3.1**). As mentioned, this was expected considering that the biomass had to consume double the FPs and the initial PHA content was higher. However, this ratio stayed low enough not to be a concern of losing selection pressure (< 0.3) (Reis et al., 2011).

Several changes were observed in the profile, higher X_a and PHA content overall, and the double increase in FPs representing the two carbon pulses are observable in **Figure 3.2 C**. During the exponential phase of the FPs consumption and conversion into PHA content, Operation 3 had a higher yield compared to previous Operations (0.66 ± 0.02 g-COD_{PHA}/g-COD_{FP} in Operation 1, 0.80 ± 0.08 g-COD_{PHA}/g-COD_{FP} in Operation 2 and 0.96 ± 0.03 g-COD_{PHA}/g-COD_{FP} in Operation 3) (**Table 3.1**), indicating a bigger conversion rate to PHA until the stationary phase was reached. As expected, there was a big increase in the PHA content during the cycle with the average during the feast doubling to 32 ± 4% (g-PHA/g-TSS) in Operation 3 in relation to Operation 1 (15 ± 4% (g-PHA/g-TSS)) and Operation 2 (13 ± 5% (g-PHA/g-TSS)), as stated in **Table 3.1**. In practical terms, the C:N ratio was strategically adjusted to 100:3.5 (C-mmol:N-mmol) by increasing the available carbon source and limiting the nitrogen supply. This stoichiometric shift was implemented to induce nutrient stress, which restricts new cell growth and redirects the high carbon flux towards intracellular PHA accumulation. This approach was designed to maximize the final polymer content in the biomass, yielding a superior polymer-rich fraction compared to prior operational strategies.

There was a new compound with a retention time similar to glucose was detected in the GC analysis of the lyophilised biomass, possibly corresponding to glycogen. It is suspected that either a change in culture allowed the proliferation of glycogen accumulating organisms (GAO) or that the excess carbon caused the culture to start deviating carbon for glycogen accumulation, Bengtsson et al. (2010) showed that PHA and glycogen accumulation in simultaneously is possible from acetic and propionic acids.

Once again, there was an increase in biomass volumetric productivity to 2.09 ± 0.04 g-X_a/(L·d) when compared to Operation 1 (0.95 ± 0.09 g-X_a/(L·d)) and Operations 2 (1.66 ± 0.02 g-X_a/(L·d)) as mentioned in **Table 3.1**.This increment occurred despite the nitrogen being supplied at the same amount as the preceding operations. Such an elevation suggests a greater efficiency of the selected culture in nitrogen and PHA consumption for growth, which is

supported by the maximum biomass yield during the PHA famine phase of 0.828 ± 0.001 g-COD_{Xa}/g-COD_{PHA}, the highest recorded among the three operations.

This feeding strategy in Operation 3 allowed the increase of the OLR to 11 g-COD/(L·d) without losing selection pressure. Previous studies that tried to increase the OLR in one volume showed a reduction in selection pressure and an increase in the FPs consumption time despite all other operating parameters and feedstocks being kept the same (Lorini et al., 2020; Matos et al., 2021b; Valentino et al., 2014). However, in the current study, the F/F ratio stayed low and selective pressure wasn't lost due to feeding the carbon in two separate pulses to avoid inhibition.

This operation demonstrated promising results towards the elimination of the accumulation step. By being able to double the OLR and maintaining the N&P volume, it was possible to increase the PHA content of the biomass after purging with approximately 40.4 ± 0.2% (g-PHA/g-TSS). With a high yield and efficient extraction process, the biomass purged from the SBR during Operation 3 could go straight to PHA extraction. However, biomasses with higher PHA contents are always desirable because the ratios are between solvent and biomass, not solvent and PHA in the biomass, which impacts the cost/benefit of the extraction because it is always preferable to use as little solvent as possible to extract as much PHA as possible. Also, higher PHA content implies smaller portions of undesirable cellular components like proteins and lipids, requiring fewer purification steps. However, this operation showed a global yield of 0.16 g-COD_{PHA}/g-COD_{FP}, which is low, and the elimination of the accumulation reactor might come at the expense of efficiency.

In summary, by purging right after the end of the feast phase, the collected biomass had higher PHA contents and neither selection pressure nor biomass yield were lost. With the two-pulse strategy, there was the intended increase in PHA content of the purged biomass.

3.2 PHA accumulation

As explained earlier, after the biomass purge in all three operations, the resulting biomass was immediately inoculated into the fed-batch accumulation reactor for PHA production. As can be observed in **Figures 3.4 A and B**, the FPs consumption and PHA accumulation profiles from Operations 1 and 2 respectively, as the cells reach their physiological storage limit, at approximately 2.28 h in Operation 1 and 2.29 in Operation 2 of the accumulation, no further significant PHA accumulation occurs, the maximum PHA stabilized at around 51 ± 3% (g-PHA/g-TSS) in Operation 1 and 53 ± 4% (g-PHA/g-TSS) as mentioned in **Table 3.2**. During the

accumulation in Operation 3, as expected, the cells reach their storage limit faster, at around 1.22 h (**Table 3.2**) after accumulation assay start, due to the fact that they started with a higher PHA content, approximately 35% (**Figure 3.4 C**), stabilizing around 51 ± 1% (g-PHA/g-TSS) as seen in **Table 3.2**.

During Operation 1, the PHA yield was 0.94 ± 0.05 g-COD_{PHA}/g-COD_{FP} and it took 7 carbon pulses until maximum PHA values were achieved (**Table 3.2**). In Operation 2, the PHA yield was slightly lower at 0.89 ± 0.04 g-COD_{PHA}/g-COD_{FP} and it took 5 carbon pulses to reach the maximum PHA content. This difference in PHA yield in Operation 2, despite small, is expected as the biomass starts the accumulation assay with a higher PHA content due to being purged after the feast phase. There was an increase in the FPs consumption rate ((-) q_{FP}) from 0.5 ± 0.1 g-COD_{FP}/(g-COD_{Xa}·h) in Operation 1 to 0.6 ± 0.2 g-COD_{FP}/(g-COD_{Xa}·h) in Operation 2, which was expected since the biomass came directly from the end of a feast phase in the SBR reactor, and was far from the maximum capacity achievable.

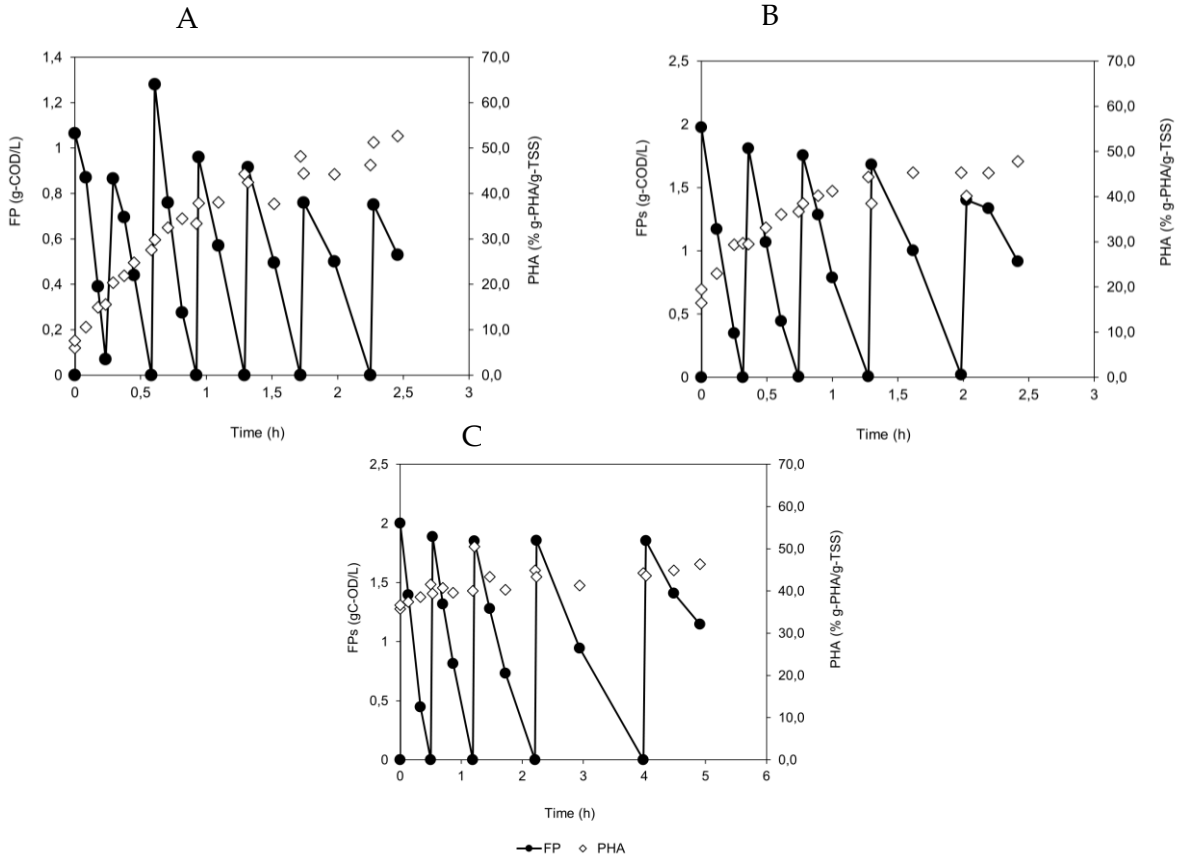

Figure 3.5- Overall PHA accumulation and FPs consumption profiles through time for accumulations done with biomass collected from SBR Operation 1 (A), Operation 2 (B) and Operation 3 (C).

Table 3.2-Summary of the controlled parameters during the accumulation monitoring. Data was displayed as Average ± SD (n=2).

Parameter	Operation 1	Operation 2	Operation 3
(-) qFP (g-COD_{FP}/g-COD_{Xa}·h)	0.5 ± 0.1	0.6 ± 0.2	0.16 ± 0.01
PHA Yield (g-COD_{PHA}/g-COD_{FP})	0.94 ± 0.05	0.89 ± 0.04	0.4 ± 0.1
Maximum PHA (% (g-PHA/g-TSS))	51 ± 3	53 ± 4	51 ± 1
Number of pulses until maximum PHA content is achieved	7	5	2
Time until maximum PHA content is achieved	2.28	2.29	1.22
Global PHA Productivity (g-PHA/(L·d))	1.18 ± 0.01	1.5 ± 0.2	2.2 ± 0.2
Global PHA yield (g-COD_{PHA}/g-COD_{FP})	0.19	0.30	0.21

The aforementioned differences in the accumulation assays for Operations 1 and 2 in this study differ from what R. A. P. Cruz et al. (2022) observed. In their work, a decrease in accumulation time from 6.6 ± 1.1 h to 4.4 ± 1.2 h and a slight increase in maximum PHA accumulation from 51% (g-PHA/g-TSS) to 56% (g-PHA/g-TSS) were noted from the traditional operation to purging after the feast, which were not the case in the present work, these differences are mainly due to their decrease in biomass in the SBR operated with the purge after the feast. In their work, the amount of carbon pulses was also very different between methodologies, with 11 for the traditional method and 3 for the biomass purged after feast. Contrary to this present work, R. A. P. Cruz et al. (2022) saw a big difference in global PHA productivity for the overall production process, while in the present study there was an increase from 1.18 ± 0.01 g-PHA/(L·d) in Operation 1 to 1.5 ± 0.2 g-PHA/(L·d) in Operation 2, they observed a reduction from 0.49 ± 0.1 g-PHA/(L·d) to 0.24 ± 0.03 g-PHA/(L·d) between the traditional method and the purge after feast, respectively, due to the decrease in biomass productivity as discussed in section 3.1. Compared to Matos et al. (2021a), our results fell short as they describe a maximum PHA content of 80.5 ± 0.3% (g-PHA/g-TSS), possibly due to the fact that they have a highly selected culture of PHA-accumulating bacteria, also, a global PHA productivity of 8.1 ± 0.1 g-PHA/(L·d) was reached due to the high PHA content obtained.

Considering these results, the biggest advantage, in terms of accumulations, between Operations 1 and 2 is in the number of carbon pulses required to achieve the maximum value of PHA content (7 in Operation 1 and 5 in Operation 2). To better evaluate the overall

performance of each operation, it is important to determine the global PHA yield (g-COD$_{PHA}$/g-COD$_{FP}$) as it represents the g-COD$_{PHA}$ produced by every g-COD$_{FP}$ consumed during the entire process from the SBR to the accumulation, helping us understand how efficiently FPs are converted into PHA. The global PHA yield showed a big increase from 0.19 g-COD$_{PHA}$/g-COD$_{FP}$ in Operation 1 to 0.30 g-COD$_{PHA}$/g-COD$_{FP}$ in Operation 2, demonstrating that purging after the end of the feast phase helps make the three-stage process overall more efficient in converting the FPs into PHA ready for extraction. Besides the PHA yield, it is also important to determine the global PHA productivity (g-PHA/(L·d)) as it allows us to determine how much PHA is produced per day. The global PHA productivity of the three-stage process increased from 1.18 ± 0.01 g-PHA/(L·d) in Operation 1 to 1.5 ± 0.2 g-PHA/(L·d) in Operation 2 due to the increase in biomass in the SBR, if there is more biomass and the g-PHA/g-TSS is the same, the PHA productivity will inevitably go up. Despite not reducing the need for the accumulation reactor, the overall need for less FPs helps make the three-stage process more attractive for the industry.

To further improve the process, a feast phase was attempted with two carbon pulses instead of the traditional one pulse. Besides the differences observed in the SBR (mentioned in point 3.1 of this thesis), there were some major differences in the accumulations, like the reduction of the time required to achieve the maximum PHA content to 1.22 hours (**Table 3.2**), which was expected considering the accumulation already started with the biomass having close to 35% (g-PHA/g-TSS) (**Figure 3.4 C**). The other noticeable impact was the number of FPs pulses needed to achieve maximum PHA content, only 2, a reduction of 5 pulses per accumulation when compared with the 7 required in Operation 1, also due to the PHA content in the beginning. The selected biomass attained a maximum PHA content of 51 ± 1% (g-PHA/g-TSS), falling in line with was observed for Operation 1 (51 ± 1% (g-PHA/g-TSS)) and Operation 2 (53 ± 4% (g-PHA/g-TSS)). As seen in the SBR monitoring of Operation 3, there was a new compound in the GC analysis of the lyophilised biomass discussed in more detail in section 3.1.

There was an increase in the global PHA productivity to 2.2 ± 0.2 g-PHA/(L·d) compared with the 1.18 ± 0.01 g-PHA/(L·d) in Operation 1 and 1.5 ± 0.2 g-PHA/(L·d) in Operation 2, caused by the big increase in biomass productivity as discussed in section 3.1. However, the global PHA yield for this operation was 0.23 g-COD$_{PHA}$/g-COD$_{FP}$, which is slightly higher than Operation 1 at 0.19 g-COD$_{PHA}$/g-COD$_{FP}$, but much lower than the 0.30 g-COD$_{PHA}$/g-COD$_{FP}$ from Operation 2. This indicates that the reduction in accumulation time and carbon pulses is being compensated by the increase in the number of carbon pulses in the SBR. Compared with

Operation 1 we might consider it a success since the PHA productivity and yield increased, even if slightly. However, when compared with Operation 2, Operation 3 is highly disadvantageous because of the lower PHA yield, and it is only more productive due to the higher biomass productivity, if this could be increased in Operation 2, it would be better in every metric evaluated in this study. A higher yield and productivity mean less costs and less waste, turning the process more attractive to industries.

In this study, the elimination of the accumulation reactor was not possible. However, Operation 2 showed the most promising results to increase the overall performance of the three-stage process. By purging after the end of the feast and maintaining the N&P volume the same as in Operation 1, we were able to increase biomass productivity inside the SBR and purge biomass with more PHA content. This higher PHA content helped to reduce the FPs products needed in the accumulation assays, which in turn increased the PHA yield and productivity.

3.3 PHA composition and properties

Besides analyzing the results obtained regarding SBR performance and PHA accumulation, it is equally important to evaluate whether the polymers produced share similar characteristics or if variations in operating conditions within the SBR influence the nature of the final polymer. This helps us understand not only the efficiency of the process but also the quality and consistency of the PHA produced, highlighting the relationship between operational parameters and polymer properties. All of the graphics from TGA, DSC and mechanical properties can be found in the **Appendix A** section.

A direct comparison between Operation 1 and Operation 2 reveals that their copolymer properties are very similar, despite the difference in SBR purge timing. Both operations result in high melting points (158.1 ± 0.7 °C in Operation 1 and 157.3 ± 0.2 °C in Operation 2), melting enthalpies (36.34 ± 1 J/g in Operation 1 and 33.4 ± 0.2 J/g in Operation 2), and crystallinity (24.9 ± 0.7% in Operation 1 and 22.9 ± 0.2% in Operation 2), with only modest differences in HV content (13.2 mol% in Operation 1 and 15.9 mol% in Operation 2) (**Table 3.3**). Mechanical properties likewise demonstrate similarity with Young's modulus of 0.4 ± 0.1 GPa and 0.43 ± 0.08 GPa but differences in UTS of 21.3 ± 0.8 MPa in Operation 1 and 15.3 ± 0.5 MPa in Operation 2, and elongations at break of 19 ± 1% and 12.3 ± 0.3% for Operations 1 and 2, respectively (**Table 3.3**), which means that the polymer from Operation 2 is less ductile. These small variations are within the expected range for PHBV copolymers produced under similar metabolic

regimes, as established in studies (Abbasi et al., 2022; Chan et al., 2019; Langford et al., 2019; Lidón Sánchez-Safont et al., 2016). However, despite being the expected range for copolymers, these differences are mainly attributed to the increased molecular weight, probably because a different MMC was selected with the change in purge timing (Hahn et al., 2024). The increase in molecular weight also increased the dispersity from 2.06 ± 0.02 in Operation 1 to 2.5 ± 0.2 in Operation 2, this implicates more short and longer chains, short chains compromise the UTS and the longer chains provide more rigidity to the polymer (Whitfield et al., 2019, 2021). Both of these changes are observed in the decreased UTS and elongation at break.

Table 3.3- Summary of the polymer properties from the 3 Operations. Data was displayed as Average ± SD (n=2).

Parameter	Operation 1	Operation 2	Operation 3
HB:HV (mol% HB:mol% HV)	86.8:13.2	84.1:15.9	79:21
Melting point (T_m, °C)	158.1 ± 0.7	157.3 ± 0.2	123.1 ± 0.2
Melting enthalpy (Δ_m, J/g)	36 ± 1	33.4 ± 0.2	14.42 ± 0.04
Melt crystallization (T_c, °C)	81.5 ± 0.4	71.25 ± 0.06	n.d.
Cold crystallization (T_{cc}, °C)	63.9 ± 0.4	69 ± 1	83.1 ± 0.3
Glass transition (T_g, °C)	1.11 ± 0.05	1.0 ± 0.4	-0.1 ± 0.3
Crystallinity (%)	24.9 ± 0.7	22.9 ± 0.2	9.88 ± 0.03
Temperature of degradation (°C)	291.7 ± 0.1	295 ± 1	289 ± 6
Temperature of 5% degradation (T_{deg}, °C)	271 ± 2	277.5 ± 0.2	266 ± 5
% mass left after total degradation	2.9 ± 0.5	3.4 ± 0.2	2.5 ± 0.2
Molecular weight (M_w, kDa)	295 ± 14	349 ± 4	341 ± 14
Dispersity ($Đ_M$)	2.06 ± 0.02	2.5 ± 0.2	2.4 ± 0.3
Young's module (E, GPa)	0.4 ± 0.1	0.43 ± 0.08	0.35 ± 0.03
Ultimate tensile strength (UTS, MPa)	21.3 ± 0.8	15.3 ± 0.5	12.9 ± 0.5
Elongation at break (ε, %)	19 ± 1	12.3 ± 0.3	18 ± 1

n.d. – Not defined, inexistent.

The crystallinity and thermal stability remain high for both, and the overall mechanical profile is closer to that of typical PHB-rich materials than to the more ductile, amorphous polymers produced under Operation 3 (Abbasi et al., 2022; Alfano et al., 2024; Chotchindakun et al., 2021).

Such close similarities reinforce the conclusion that, under these operational conditions and with consistent precursor profiles, purging either after famine or after feast generates

copolymers with comparable structure and performance, offering flexibility in process scheduling without impacting the material's final properties.

A progressive increase in HV content from Operation 1 (86.8:13.2 mol% HB:mol% HV) to Operation 3 (79:21 mol% HB:mol% HV) is observed despite maintaining the HB:HV precursors ratio in all operations, which is accompanied by marked changes in the material's structural and performance characteristics (**Table 3.3**). Specifically, the melting point decreases substantially from 158.1 ± 0.7 °C in Operation 1 to 123.1 ± 0.2 °C in Operation 3, and the melting enthalpy also drops sharply, indicating a reduction in overall crystallinity as HV monomers are increasingly incorporated into the copolymer chain, these results are in line with what other studies observed for the reduction in melt temperature with the increase in HV (**Table 3.3**) (Abbasi et al., 2022; Alfano et al., 2024; Chan et al., 2019; Wang et al., 2013).

When calculated, crystallinity drops from 24.9 ± 0.7% in Operation 1 to just 9.88 ± 0.03% in Operation 3, which is consistent with literature reports demonstrating that increasing HV content can result in a more disordered polymer structure and reduced crystalline domain formation (Abbasi et al., 2022; Lidón Sánchez-Safont et al., 2016). For example, pure PHB typically exhibits crystallinity values between 53% and 68%, whereas PHBV copolymers containing 8 mol% HV can display crystallinity as low as 4.8%, PHBV with 10–30 mol% HV generally show values in the 10–40% range (Abbasi et al., 2022; Barbosa et al., 2021; Langford et al., 2019). These variations reinforce the results observed, highlighting that higher HV incorporation diminishes the order and size of crystalline domains in these biopolymers (**Table 3.3**).

These thermal trends are further reflected in the glass transition temperature, which falls below zero for the sample with the highest HV content, indicating a more amorphous polymer matrix typical of HV-rich PHBV copolymers (Abbasi et al., 2022; Barbosa et al., 2021) (**Table 3.3**).

Thermal degradation behavior shows a slight decrease in stability as HV content rises, but all samples retain relatively high temperatures of onset, ranging from 295 ± 1 °C down to 289 ± 6 °C (**Table 3.3**). This modest reduction in thermal stability parallels published studies on PHBV, which report similar tendencies as the copolymer becomes more amorphous and flexible (Abbasi et al., 2022; Conceição et al., 2023; Lidón Sánchez-Safont et al., 2016).

The mechanical properties support these structural observations as Young's modulus decreases from 0.4 ± 0.1 GPa in Operation 1 to 0.35 ± 0.03 GPa in Operation 3, and the UTS drops from 21.3 ± 0.8 MPa to 12.9 ± 0.5 MPa (**Table 3.3**). Literature reports for PHBV copolymers show Young's modulus values between 0.2 and 0.7 GPa and UTS between 10 and 25 MPa,

aligning well with the present data (Alfano et al., 2024; Rivera-Briso & Serrano-Aroca, 2018; Tomano et al., 2022). As observed in Operation 2, there was an increase in molecular weight and dispersity to 341 ± 14 kDa and 2.4 ± 0.3, respectively, when compared to Operation 1. Most notably, elongation at break increases from 12.3 ± 0.3% at the lower HV content to 19 ± 1% at the highest, confirming that HV-rich copolymers are substantially tougher and less brittle, a trend commonly observed in the literature, with studies reporting elongation at break from 15% up to 130% for copolymers with HV content above 20% (**Table 3.3)** (Abbasi et al., 2022; Chotchindakun et al., 2021).

The increases in molecular weight and dispersity, coupled with the increase in HV content explain the reduction in UTS and increase in elongation at break as increasing HV content typically reduces stiffness and strength due to more interrupted crystalline packing but imparts greater ductility to the material (Abbasi et al., 2022; Chotchindakun et al., 2021).

While the precise values can depend on microstructure, processing, and test conditions, these results broadly agree with the established property ranges for PHBV copolymers produced in SBR systems and support the role of operational regime as a powerful modifier of material performance.

4

CONCLUSIONS AND FUTURE WORK

In order to assess the impact of the purge timing and the carbon feeding strategy on the PHA production process using mixed microbial cultures and a real feedstock (apple pulp waste), three operational strategies were tested in the selection reactor of a typical three-stage process implemented at pilot scale. Operation 1 followed the traditional cycle approach, starting with the feast phase, followed by famine, and purging after the famine phase. Operation 2 applied the purge immediately after the feast phase, before the addition of N&P, thereby evaluating the effect of purge timing in relation to the physiological state of the biomass. Finally, in Operation 3, a two-pulse feeding strategy was combined with the purge after the feast phase, aiming to increase the PHA content at the time of purging without causing inhibition by carbon excess.

In the traditional Operation 1, the biomass purged from the reactor had 11.8 ± 0.1% (g-PHA/g-TSS) and a biomass productivity of 1.3 ± 0.1 g-X_a/(L·d). After 7 carbon pulses, the maximum PHA content was 51 ± 3% (g-PHA/g-TSS) with an overall PHA yield of 0.19 g-COD_{PHA}/g-COD_{FP}, and an overall PHA productivity of 1.18 ± 0.01 g-PHA/(L·d). This Operation 1 was used as a benchmark for comparison with Operations 2 and 3.

It was observed in Operation 2 that the biomass exiting the SBR had an intracellular PHA content of 19.9 ± 0.5% (g-PHA/g-TSS), initiating the accumulation phase with more PHA than the traditional configuration, therefore needing only 5 carbon pulses until a maximum PHA content of 53 ± 4% (g-PHA/g-TSS) was achieved. The global PHA productivity and yield also increased by purging biomass at the end of the feast phase to 1.5 ± 0.2 g-PHA/(L·d) and 0.30 g-COD_{PHA}/g-COD_{FP}, respectively. The PHA productivity increased due to the increase of biomass productivity to 1.66 ± 0.02 g-X_a/(L·d) and the PHA yield increased due to the decreased number of carbon pulses required in the accumulation assays. Moreover, compared with the polymer from Operation 1, there were no significant alterations observed in the polymer's composition and properties, indicating no substantial metabolic changes from shifting the purge timing within the SBR.

With the two-pulse feeding strategy in Operation 3, as expected, there was an increase in the maximum PHA content during the feast to 40.4 ± 0.2% (g-PHA/g-TSS), which translated into a shorter accumulation and only 2 carbon pulses until a maximum of 51 ± 1% (g-PHA/g-TSS) was reached. The global PHA productivity, compared to Operations 1 and 2, increased due to the increase in biomass productivity to 2.09 ± 0.04 g-X_a/(L·d). However, the global PHA yield decreased to 0.21 g-COD_{PHA}/g-COD_{FP} due to the increase in FPs needed for the SBR, which is a big disadvantage because it significantly increases raw material costs, reduces process efficiency and compromises its economic and environmental viability on an industrial scale. In this case, a metabolic shift was observed in the culture, leading to a change in the polymer composition. The polymer produced contained a higher HV mol% even though the feedstock had the same precursor ratio for HB and HV, which in turn altered the physical and mechanical properties of the polymer.

To conclude, Operation 2 proved to be the best option as it was possible to reduce the volume of the UASB reactor required since a lower volume of FPs is needed to run the overall system, this reduces the operating and maintenance costs associated with bigger volumes, facilitating the process.

For future work, it is suggested that a microbial population analysis should be performed to better understand if and how the different operating strategies impacted the MMC composition and its relation with the results obtained. As the increase of the OLR in Operation 3 did not cause inhibition, it is suggested to also increase the C:N ratio to match the carbon fed, this could help increase the biomass productivity, which in turn might increase the overall PHA productivity and yield as the accumulation reactor is inoculated with more biomass. At last, shortening the famine phase might decrease the PHA consumption for cell maintenance, however, if too shortened it can cause the loss of the selection pressure induced by the starvation period.

REFERENCES

Abbasi, M., Pokhrel, D., Coats, E. R., Guho, N. M., & McDonald, A. G. (2022). Effect of 3-Hydroxyvalerate Content on Thermal, Mechanical, and Rheological Properties of Poly(3-hydroxybutyrate-co-3-hydroxyvalerate) Biopolymers Produced from Fermented Dairy Manure. *Polymers*, *14*(19), 4140. https://doi.org/10.3390/POLYM14194140/S1

Achakulwisut, P., Erickson, P., Guivarch, C., Schaeffer, R., Brutschin, E., & Pye, S. (2023). Global fossil fuel reduction pathways under different climate mitigation strategies and ambitions. *Nature Communications 2023 14:1*, *14*(1), 1–15. https://doi.org/10.1038/s41467-023-41105-z

Afreen, R., Tyagi, S., Singh, G. P., & Singh, M. (2021). Challenges and Perspectives of Polyhydroxyalkanoate Production From Microalgae/Cyanobacteria and Bacteria as Microbial Factories: An Assessment of Hybrid Biological System. *Frontiers in Bioengineering and Biotechnology*, *9*, 624885. https://doi.org/10.3389/FBIOE.2021.624885/XML

Albuquerque, M. G. E., Bengtsson, S., Martino, V., Pollet, E., & Reis, M. A. M. (2010). Eco-engineering of mixed microbial cultures to develop a cost-effective bioplastic (PHA) production process from a surplus feedstock — sugar molasses. *Journal of Biotechnology*, *150*, 70. https://doi.org/10.1016/J.JBIOTEC.2010.08.183

Alfano, S., Doineau, E., Perdrier, C., Preziosi-Belloy, L., Gontard, N., Martinelli, A., Grousseau, E., & Angellier-Coussy, H. (2024). Influence of the 3-Hydroxyvalerate Content on the Processability, Nucleating and Blending Ability of Poly(3-Hydroxybutyrate-co-3-hydroxyvalerate)-Based Materials. *ACS Omega*, *9*(27), 29360–29371. https://doi.org/10.1021/ACSOMEGA.4C01282

Alfano, S., Lorini, L., Majone, M., Sciubba, F., Valentino, F., & Martinelli, A. (2021). Ethylic Esters as Green Solvents for the Extraction of Intracellular Polyhydroxyalkanoates Produced by Mixed Microbial Culture. *Polymers 2021, Vol. 13, Page 2789*, *13*(16), 2789. https://doi.org/10.3390/POLYM13162789

https://doi.org/10.3390/POLYM13162789

Bagatella, S., Ciapponi, R., Ficara, E., Frison, N., & Turri, S. (2022). Production and Characterization of Polyhydroxyalkanoates from Wastewater via Mixed Microbial Cultures and Microalgae. *Sustainability 2022, Vol. 14, Page 3704*, *14*(6), 3704. https://doi.org/10.3390/SU14063704

Barbosa, J. L., Perin, G. B., & Felisberti, M. I. (2021). Plasticization of Poly(3-hydroxybutyrate-co-3-hydroxyvalerate) with an Oligomeric Polyester: Miscibility and Effect of the Microstructure and Plasticizer Distribution on Thermal and Mechanical Properties. *ACS Omega*, *6*(4), 3278–3290. https://doi.org/10.1021/ACSOMEGA.0C05765

Bedade, D. K., Edson, C. B., & Gross, R. A. (2021). Emergent Approaches to Efficient and Sustainable Polyhydroxyalkanoate Production. *Molecules 2021, Vol. 26, Page 3463*, *26*(11), 3463. https://doi.org/10.3390/MOLECULES26113463

Bengtsson, S., Pisco, A. R., Reis, M. A. M., & Lemos, P. C. (2010). Production of polyhydroxyalkanoates from fermented sugar cane molasses by a mixed culture enriched in glycogen accumulating organisms. *Journal of Biotechnology*, *145*(3), 253–263. https://doi.org/10.1016/J.JBIOTEC.2009.11.016

Bravo-Porras, G., Fernández-Güelfo, L. A., Álvarez-Gallego, C. J., Carbú, M., Sales, D., & Romero-García, L. I. (2024). Influence of the total concentration and the profile of volatile fatty acids on polyhydroxyalkanoates (PHA) production by mixed microbial cultures. *Biomass Conversion and Biorefinery*, *14*(1), 239–253. https://doi.org/10.1007/S13399-021-02208-Z/FIGURES/2

Carvalho, J. M., Marreiros, B. C., & Reis, M. A. M. (2022). Polyhydroxyalkanoates Production by Mixed Microbial Culture under High Salinity. *Sustainability (Switzerland)*, *14*(3), 1346. https://doi.org/10.3390/SU14031346/S1

Castagnoli, A., Falcioni, S., Touloupakis, E., Pasciucco, F., Pasciucco, E., Michelotti, A., Iannelli, R., & Pecorini, I. (2024). Influence of Aeration Rate on

Uncoupled Fed Mixed Microbial Cultures for Polyhydroxybutyrate Production. *Sustainability 2024, Vol. 16, Page 2961*, *16*(7), 2961. https://doi.org/10.3390/SU16072961

Chan, C. M., Vandi, L. J., Pratt, S., Halley, P., Ma, Y., Chen, G. Q., Richardson, D., Werker, A., & Laycock, B. (2019). Understanding the effect of copolymer content on the processability and mechanical properties of polyhydroxyalkanoate (PHA)/wood composites. *Composites Part A: Applied Science and Manufacturing*, *124*, 105437. https://doi.org/10.1016/J.COMPOSITESA.2019.05.005

Chotchindakun, K., Pathom-aree, W., Dumri, K., Ruangsuriya, J., Pumas, C., & Pekkoh, J. (2021). Low Crystallinity of Poly(3-Hydroxybutyrate-co-3-Hydroxyvalerate) Bioproduction by Hot Spring Cyanobacterium Cyanosarcina sp. AARL T020. *Plants 2021, Vol. 10, Page 503*, *10*(3), 503. https://doi.org/10.3390/PLANTS10030503

Clesceri, L. S. ., Eaton, A. D. ., & Greenberg, A. E. . (1999). *Standard Methods for the Examination of Water and Wastewater Edition: 20th Edition*. American Public Health Association (APHA).

Colombo, B., Favini, F., Scaglia, B., Sciarria, T. P., D'Imporzano, G., Pognani, M., Alekseeva, A., Eisele, G., Cosentino, C., & Adani, F. (2017). Enhanced polyhydroxyalkanoate (PHA) production from the organic fraction of municipal solid waste by using mixed microbial culture. *Biotechnology for Biofuels*, *10*(1), 1–15. https://doi.org/10.1186/S13068-017-0888-8/TABLES/6

Conceição, M. N., dos Santos, M. C. C., Mancipe, J. M. A., Pereira, P. S. C., Ribeiro, R. C. C., Thiré, R. M. S. M., & Bastos, D. C. (2023). A Biodegradable Composite of Poly (3-hydroxybutyrate-co-3-hydroxyvalerate) (PHBV) with Short Cellulose Fiber for Packaging. *Materials Research*, *26*(suppl 1), e20220615. https://doi.org/10.1590/1980-5373-MR-2022-0615

Costa, A., Encarnação, T., Tavares, R., Todo Bom, T., & Mateus, A. (2023). Bioplastics: Innovation for Green Transition. *Polymers 2023, Vol. 15, Page 517*, *15*(3), 517. https://doi.org/10.3390/POLYM15030517

Cruz, R. A. P., Oehmen, A., & Reis, M. A. M. (2022). The impact of biomass withdrawal strategy on the biomass selection and polyhydroxyalkanoates

accumulation of mixed microbial cultures. *New Biotechnology*, *66*, 8–15. https://doi.org/10.1016/J.NBT.2021.08.004

Cruz, R. M. S., Krauter, V., Krauter, S., Agriopoulou, S., Weinrich, R., Herbes, C., Scholten, P. B. V., Uysal-Unalan, I., Sogut, E., Kopacic, S., Lahti, J., Rutkaite, R., & Varzakas, T. (2022). Bioplastics for Food Packaging: Environmental Impact, Trends and Regulatory Aspects. *Foods 2022, Vol. 11, Page 3087*, *11*(19), 3087. https://doi.org/10.3390/FOODS11193087

Duque, A. F., Oliveira, C. S. S., Carmo, I. T. D., Gouveia, A. R., Pardelha, F., Ramos, A. M., & Reis, M. A. M. (2014). Response of a three-stage process for PHA production by mixed microbial cultures to feedstock shift: impact on polymer composition. *New Biotechnology*, *31*(4), 276–288. https://doi.org/10.1016/J.NBT.2013.10.010

Folino, A., Karageorgiou, A., Calabrò, P. S., & Komilis, D. (2020). Biodegradation of Wasted Bioplastics in Natural and Industrial Environments: A Review. *Sustainability 2020, Vol. 12, Page 6030*, *12*(15), 6030. https://doi.org/10.3390/SU12156030

Getino, L., Martín, J. L., & Chamizo-Ampudia, A. (2024). A Review of Polyhydroxyalkanoates: Characterization, Production, and Application from Waste. *Microorganisms 2024, Vol. 12, Page 2028*, *12*(10), 2028. https://doi.org/10.3390/MICROORGANISMS12102028

Gontard, N., Sonesson, U., Birkved, M., Majone, M., Bolzonella, D., Celli, A., Angellier-Coussy, H., Jang, G.-W., Verniquet, A., Broeze, J., Schaer, B., Paula Batista, A., & Sebok, A. (2022). An Overview on Wood Waste Valorization as Biopolymers and Biocomposites: Definition, Classification, Production, Properties and Applications. *Polymers 2022, Vol. 14, Page 5519*, *14*(24), 5519. https://doi.org/10.3390/POLYM14245519

Gujer, W., & Henze, M. (1991). Activated Sludge Modelling and Simulation. *Water Science and Technology*, *23*(4–6), 1011–1023. https://doi.org/10.2166/WST.1991.0553

Guzik, M. W. (2021). Polyhydroxyalkanoates, bacterially synthesized polymers, as a source of chemical compounds for the synthesis of advanced materials and bioactive molecules. *Applied Microbiology and Biotechnology*, *105*(20), 7555–7566. https://doi.org/10.1007/S00253-021-11589-0/FIGURES/4

Hahn, T., Alzate, M. O., Leonhardt, S., Tamang, P., & Zibek, S. (2024). Current trends in medium-chain-length polyhydroxyalkanoates: Microbial production, purification, and characterization. *Engineering in Life Sciences*, *24*(6), 2300211. https://doi.org/10.1002/ELSC.202300211;JOURNAL:JOURNAL:15213846;WGROUP:STRING:PUBLICATION

Jiang, M., Cao, Y., Liu, C., Chen, D., Zhou, W., Wen, Q., Yu, H., Jiang, J., Ren, Y., Hu, S., Hertwich, E., & Zhu, B. (2024). Tracing fossil-based plastics, chemicals and fertilizers production in China. *Nature Communications*, *15*(1), 1–12. https://doi.org/10.1038/S41467-024-47930-0;SUBJMETA

Jin, A., del Valle, L. J., & Puiggalí, J. (2023). Copolymers and Blends Based on 3-Hydroxybutyrate and 3-Hydroxyvalerate Units. *International Journal of Molecular Sciences 2023, Vol. 24, Page 17250*, *24*(24), 17250. https://doi.org/10.3390/IJMS242417250

Kalia, V. C., Patel, S. K. S., & Lee, J. K. (2023). Exploiting Polyhydroxyalkanoates for Biomedical Applications. *Polymers 2023, Vol. 15, Page 1937*, *15*(8), 1937. https://doi.org/10.3390/POLYM15081937

Kalia, V. C., Singh, R. V., Gong, C., & Lee, J. K. (2025). Toward Sustainable Polyhydroxyalkanoates: A Next-Gen Biotechnology Approach. *Polymers 2025, Vol. 17, Page 853*, *17*(7), 853. https://doi.org/10.3390/POLYM17070853

Koller, M. (2018). Biodegradable and Biocompatible Polyhydroxy-alkanoates (PHA): Auspicious Microbial Macromolecules for Pharmaceutical and Therapeutic Applications. *Molecules 2018, Vol. 23, Page 362*, *23*(2), 362. https://doi.org/10.3390/MOLECULES23020362

Kshirsagar, A. B., Shinde, A. A., Kshirsagar, A. B., & Shinde, A. A. (2023). Bioplastic from renewable biomass sources. *International Journal of Science and Research Archive*, *8*(1), 225–235. https://doi.org/10.30574/IJSRA.2023.8.1.0012

Langford, A., Chan, C. M., Pratt, S., Garvey, C. J., & Laycock, B. (2019). The morphology of crystallisation of PHBV/PHBV copolymer blends. *European Polymer Journal*, *112*, 104–119. https://doi.org/10.1016/J.EURPOLYMJ.2018.12.022

Lelieveld, J., Haines, A., Burnett, R., Tonne, C., Klingmüller, K., Münzel, T., & Pozzer, A. (2023). Air pollution deaths attributable to fossil fuels:

observational and modelling study. *BMJ*, *383*. https://doi.org/10.1136/BMJ-2023-077784

Lidón Sánchez-Safont, E., González-Ausejo, J., Gámez-Pérez, J., María Lagarón, J., & Cabedo, L. (2016). Poly(3-Hydroxybutyrate-co-3-Hydroxyvalerate)/ Purifi ed Cellulose Fiber Composites by Melt Blending: Characterization and Degradation in Composting Conditions. *J. Renew. Mater*, *4*(2). https://doi.org/10.7569/JRM.2015.634127

Lorini, L., di Re, F., Majone, M., & Valentino, F. (2020). High rate selection of PHA accumulating mixed cultures in sequencing batch reactors with uncoupled carbon and nitrogen feeding. *New Biotechnology*, *56*, 140–148. https://doi.org/10.1016/J.NBT.2020.01.006

Maestro, B., & Sanz, J. M. (2017). Polyhydroxyalkanoate-associated phasins as phylogenetically heterogeneous, multipurpose proteins. *Microbial Biotechnology*, *10*(6), 1323–1337. https://doi.org/10.1111/1751-7915.12718;CSUBTYPE:STRING:SPECIAL;PAGE:STRING:ARTICLE/CHAPTER

Matos, M., Cruz, R. A. P., Cardoso, P., Silva, F., Freitas, E. B., Carvalho, G., & Reis, M. A. M. (2021a). Combined Strategies to Boost Polyhydroxyalkanoate Production from Fruit Waste in a Three-Stage Pilot Plant. *ACS Sustainable Chemistry and Engineering*, *9*(24), 8270–8279. https://doi.org/10.1021/ACSSUSCHEMENG.1C02432/SUPPL_FILE/SC1C02432_SI_001.PDF

Matos, M., Cruz, R. A. P., Cardoso, P., Silva, F., Freitas, E. B., Carvalho, G., & Reis, M. A. M. (2021b). Sludge retention time impacts on polyhydroxyalkanoate productivity in uncoupled storage/growth processes. *Science of the Total Environment*, *799*. https://doi.org/10.1016/j.scitotenv.2021.149363

Maurya, P. K., Mondal, S., Kumar, V., & Singh, S. P. (2021). Roadmap to sustainable carbon-neutral energy and environment: can we cross the barrier of biomass productivity? *Environmental Science and Pollution Research*, *28*(36), 49327–49342. https://doi.org/10.1007/S11356-021-15540-8/FIGURES/8

Mittendorf, V., Robertson, E. J., Leech, R. M., Krüger, N., Steinbüchel, A., & Poirier, Y. (1998). Synthesis of medium-chain-length polyhydroxyalkanoates in Arabidopsis thaliana using intermediates of peroxisomal fatty acid β-oxidation. *Proceedings of the National Academy of Sciences of the United States of*

America, *95*(23), 13397–13402. https://doi.org/10.1073/PNAS.95.23.13397/ASSET/764D3C1D-7AA3-4CCF-B868-6178E3A94120/ASSETS/GRAPHIC/PQ2383556004.JPEG

Mohamued, E. A., Ahmed, M., Pypłacz, P., Liczmańska-Kopcewicz, K., & Khan, M. A. (2021). Global Oil Price and Innovation for Sustainability: The Impact of R&D Spending, Oil Price and Oil Price Volatility on GHG Emissions. *Energies 2021, Vol. 14, Page 1757*, *14*(6), 1757. https://doi.org/10.3390/EN14061757

Morgan-Sagastume, F. (2016). Characterisation of open, mixed microbial cultures for polyhydroxyalkanoate (PHA) production. *Reviews in Environmental Science and Biotechnology*, *15*(4), 593–625. https://doi.org/10.1007/S11157-016-9411-0/TABLES/3

Mukherjee, M. ;, Koller, A. ;, What, M., Bioplastics, A. ", Álvarez-Castillo, E., Bengoechea, C., Guerrero, A., Lackner, M., Mukherjee, A., & Koller, M. (2023). What Are "Bioplastics"? Defining Renewability, Biosynthesis, Biodegradability, and Biocompatibility. *Polymers 2023, Vol. 15, Page 4695*, *15*(24), 4695. https://doi.org/10.3390/POLYM15244695

Neofytou, H., Karakosta, C., & Gómez, N. C. (2018). Impact assessment of climate and energy policy scenarios: A multi-criteria approach. *Understanding Risks and Uncertainties in Energy and Climate Policy: Multidisciplinary Methods and Tools for a Low Carbon Society*, 123–142. https://doi.org/10.1007/978-3-030-03152-7_5/TABLES/15

Rangel, C., Carvalho, G., Oehmen, A., Frison, N., Lourenço, N. D., & Reis, M. A. M. (2023). Polyhydroxyalkanoates production from ethanol- and lactate-rich fermentate of confectionary industry effluents. *International Journal of Biological Macromolecules*, *229*, 713–723. https://doi.org/10.1016/J.IJBIOMAC.2022.12.268

Reis, M., Albuquerque, M., Villano, M., & Majone, M. (2011). Mixed Culture Processes for Polyhydroxyalkanoate Production from Agro-Industrial Surplus/Wastes as Feedstocks. *Comprehensive Biotechnology, Second Edition*, *6*, 669–683. https://doi.org/10.1016/B978-0-08-088504-9.00464-5

Rhodes, C. J. (2018). Plastic Pollution and Potential Solutions. *Science Progress*, *101*(3), 207–260. https://doi.org/10.3184/003685018X15294876706211

Rivera-Briso, A. L., & Serrano-Aroca, Á. (2018). Poly(3-Hydroxybutyrate-co-3-Hydroxyvalerate): Enhancement Strategies for Advanced Applications. *Polymers 2018, Vol. 10, Page 732*, *10*(7), 732. https://doi.org/10.3390/POLYM10070732

Roman, D. L., Isvoran, A., Filip, M., Ostafe, V., & Zinn, M. (2020). In silico Assessment of Pharmacological Profile of Low Molecular Weight Oligo-Hydroxyalkanoates. *Frontiers in Bioengineering and Biotechnology*, *8*, 584010. https://doi.org/10.3389/FBIOE.2020.584010/BIBTEX

Schernikau, L., & Smith, W. H. (2022). Climate impacts of fossil fuels in todays electricity systems. *Journal of the Southern African Institute of Mining and Metallurgy*, *122*(3), 133–145. https://doi.org/10.17159/2411-9717/1874/2022

Serafim, L. S., Lemos, P. C., Torres, C., Reis, M. A. M., & Ramos, A. M. (2008). The influence of process parameters on the characteristics of polyhydroxyalkanoates produced by mixed cultures. *Macromolecular Bioscience*, *8*(4), 355–366. https://doi.org/10.1002/MABI.200700200;WEBSITE:WEBSITE:PERICLES;WGROUP:STRING:PUBLICATION

Sergeant, M. (2024). Turn off the tap! *Canadian Family Physician*, *70*(4), 271–273. https://doi.org/10.46747/CFP.7004271

Tábi, T. (2022). Biodegradable bio-based plastics: Compostable or recyclable? *Express Polymer Letters*, *16*(2), 115. https://doi.org/10.3144/EXPRESSPOLYMLETT.2022.9

Thorat Gadgil, B. S., Killi, N., & Rathna, G. V. N. (2017). Polyhydroxyalkanoates as biomaterials. *MedChemComm*, *8*(9), 1774–1787. https://doi.org/10.1039/C7MD00252A

Tomano, N., Boondamnoen, O., Aumnate, C., & Potiyaraj, P. (2022). Enhancing impact resistance and biodegradability of PHBV by melt blending with ENR. *Scientific Reports*, *12*(1), 1–14. https://doi.org/10.1038/S41598-022-27246-Z;SUBJMETA

Valentino, F., Beccari, M., Fraraccio, S., Zanaroli, G., & Majone, M. (2014). Feed frequency in a Sequencing Batch Reactor strongly affects the production of polyhydroxyalkanoates (PHAs) from volatile fatty acids. *New Biotechnology*, *31*(4), 264–275. https://doi.org/10.1016/j.nbt.2013.10.006

Valentino, F., Riccardi, C., Campanari, S., Pomata, D., & Majone, M. (2015). Fate of β-hexachlorocyclohexane in the mixed microbial cultures (MMCs) three-stage polyhydroxyalkanoates (PHA) production process from cheese whey. *Bioresource Technology*, *192*, 304–311. https://doi.org/10.1016/J.BIORTECH.2015.05.083

Wang, Y., Chen, R., Cai, J. Y., Liu, Z., Zheng, Y., Wang, H., Li, Q., & He, N. (2013). Biosynthesis and Thermal Properties of PHBV Produced from Levulinic Acid by Ralstonia eutropha. *PLOS ONE*, *8*(4), e60318. https://doi.org/10.1371/JOURNAL.PONE.0060318

What is the difference between biobased and biodegradable plastics? – INGREEN. (n.d.). Retrieved September 28, 2025, from https://ingreenproject.eu/what-is-the-difference-between-biobased-and-biodegradable-plastics/

Whitfield, R., Truong, N. P., & Anastasaki, A. (2021). Precise Control of Both Dispersity and Molecular Weight Distribution Shape by Polymer Blending. *Angewandte Chemie International Edition*, *60*(35), 19383–19388. https://doi.org/10.1002/ANIE.202106729

Whitfield, R., Truong, N. P., Messmer, D., Parkatzidis, K., Rolland, M., & Anastasaki, A. (2019). Tailoring polymer dispersity and shape of molecular weight distributions: methods and applications. *Chemical Science*, *10*(38), 8724–8734. https://doi.org/10.1039/C9SC03546J

Wongsirichot, P. (2025). Pilot scale polyhydroxyalkanoates biopolymer production using pure cultures: current status and future opportunities. *Critical Reviews in Biotechnology*, *45*(4), 887–903. https://doi.org/10.1080/07388551.2024.2409112

Yang, L., Tang, J., Tchounwou, P. B., Deng, C., Guo, Z., Huang, X., & Shen, T. (2023). The Dynamic Nexus of Fossil Energy Consumption, Temperature and Carbon Emissions: Evidence from Simultaneous Equation Model. *International Journal of Environmental Research and Public Health 2023, Vol. 20, Page 2042*, *20*(3), 2042. https://doi.org/10.3390/IJERPH20032042

Ye, H. Y. (2024). The Transformation of Biomass to Bio-nature Gas, Principles and Future Development Trends. *Highlights in Science, Engineering and Technology*, *83*, 790–795. https://doi.org/10.54097/0FQANN87

Yusuf, M., & Abdullah, B. (2020). Fossil Fuels, Rising Population, and Global Warming: The Interlinked Phenomena. *Oriental Journal of Physical Sciences*, *5*(1–2), 49–52. https://doi.org/10.13005/OJPS05.01-02.07

A

APPENDIX

A.1 Graphics from DSC analyses

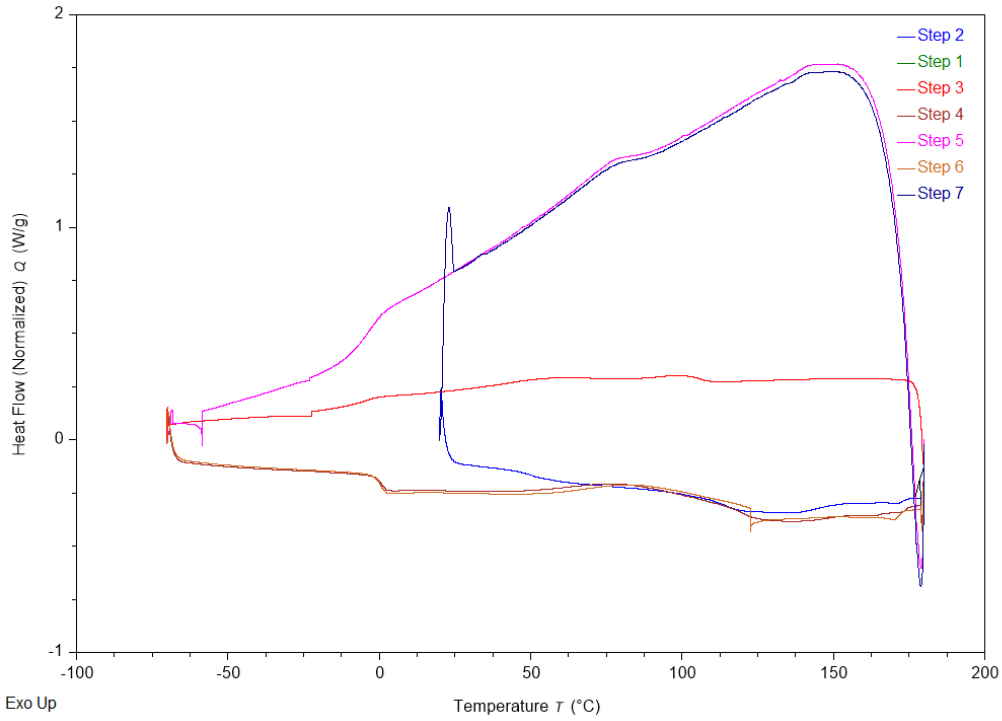

Figure A.1-DSC graphic of sample 1 from Operation 1 with the 7 analysis steps.

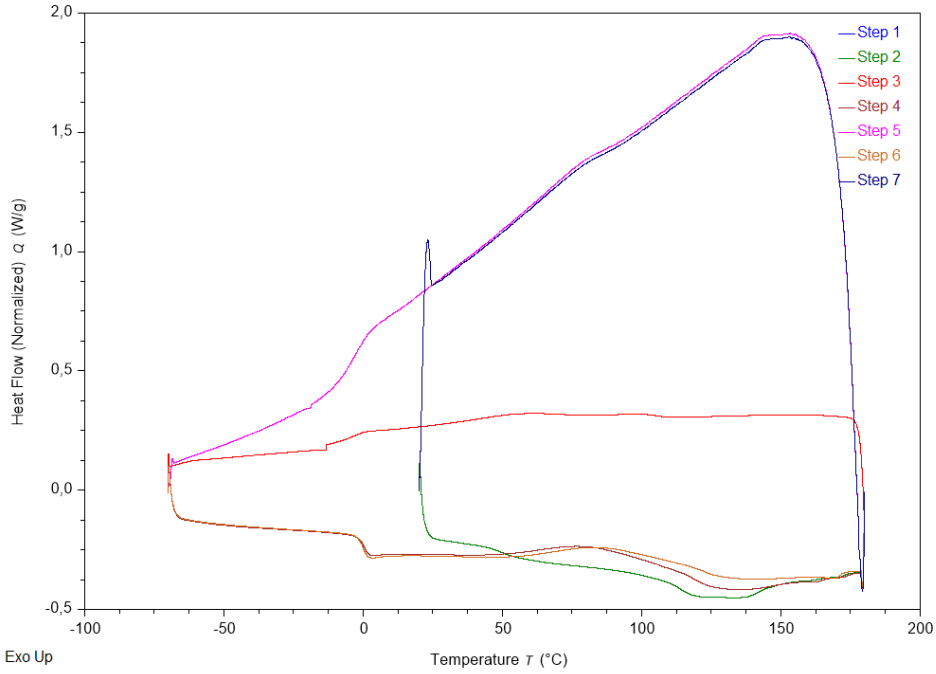

Figure A.2-DSC graphic of sample 2 from Operation 1 with the 7 analysis steps.

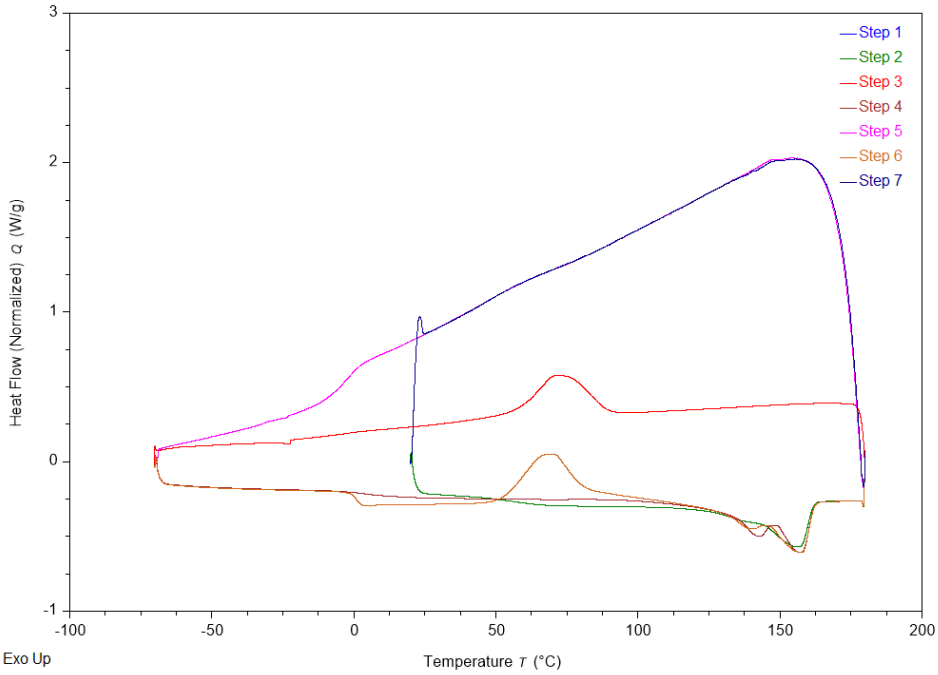

Figure A.3-DSC graphic of sample 1 from Operation 2 with the 7 analysis steps.

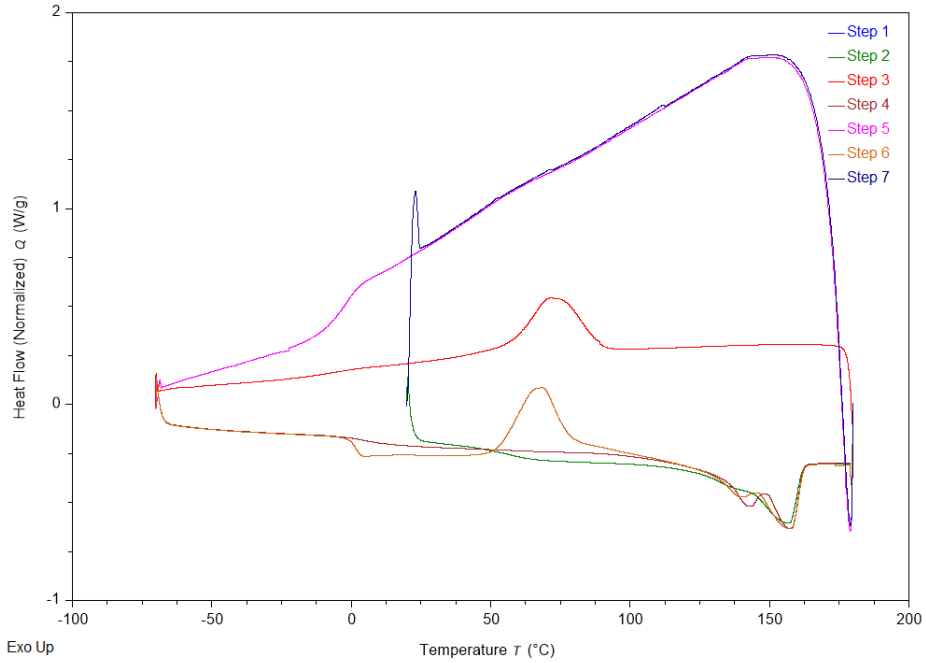

Figure A.4-DSC graphic of sample 2 from Operation 2 with the 7 analysis steps.

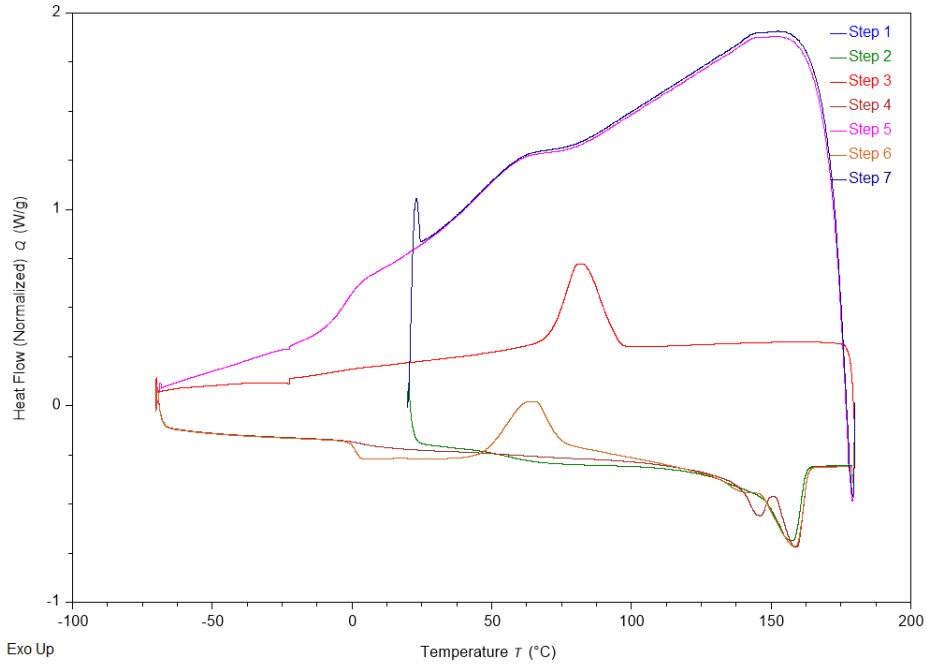

Figure A.5-DSC graphic of sample 1 from Operation 3 with the 7 analysis steps.

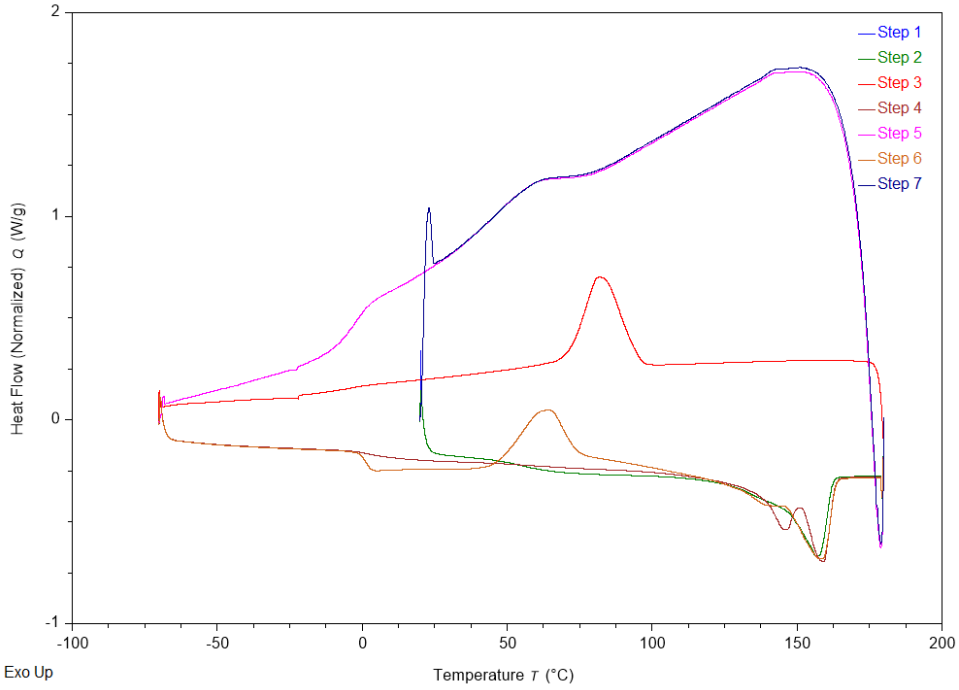

Figure A.6-DSC graphic of sample 2 from Operation 3 with the 7 analysis steps.

A.2 Graphics from TGA analyses

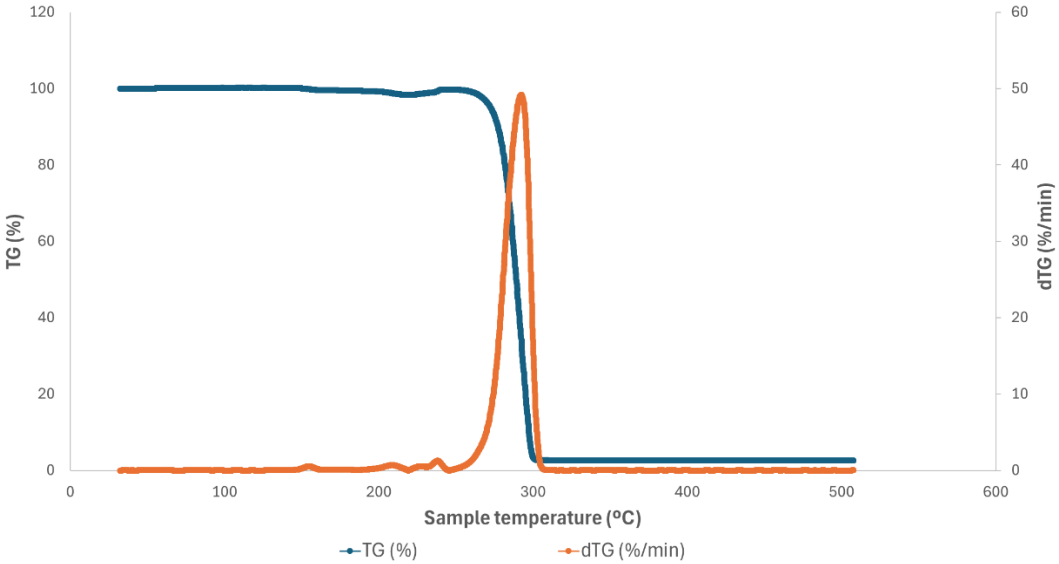

Figure A.7-TGA graphic of sample 1 from Operation 1 with TG (%) and dTG (%/min).

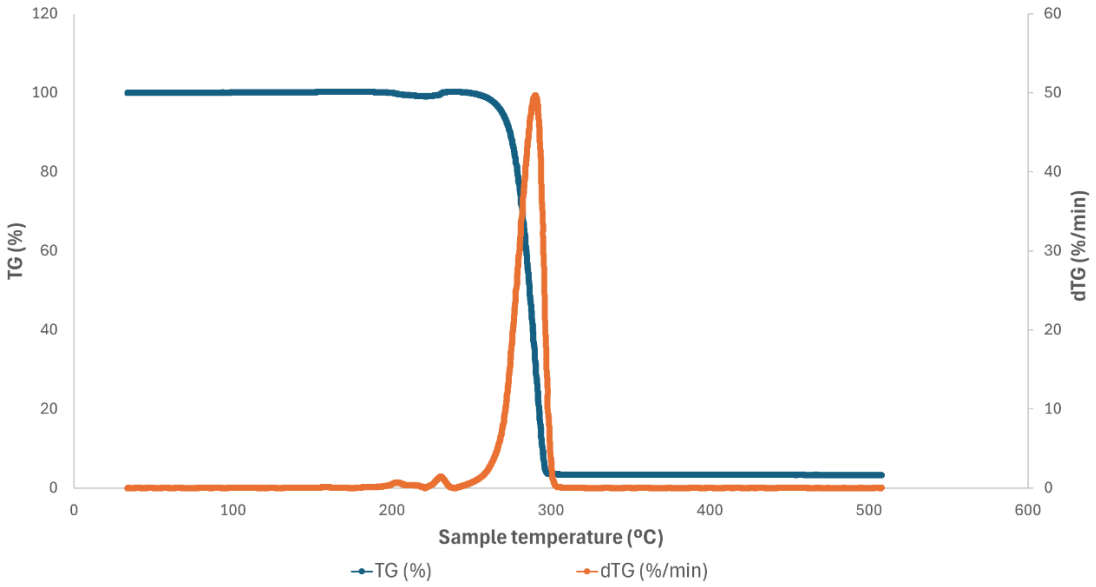

Figure A.8-TGA graphic of sample 2 from Operation 1 with TG (%) and dTG (%/min).

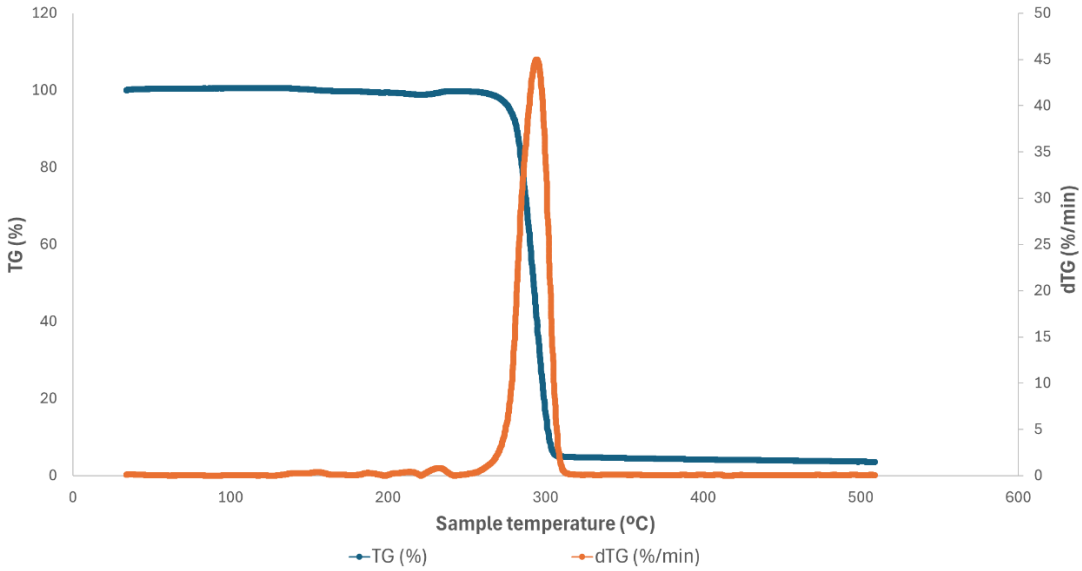

Figure A.9-TGA graphic of sample 1 from Operation 2 with TG (%) and dTG (%/min).

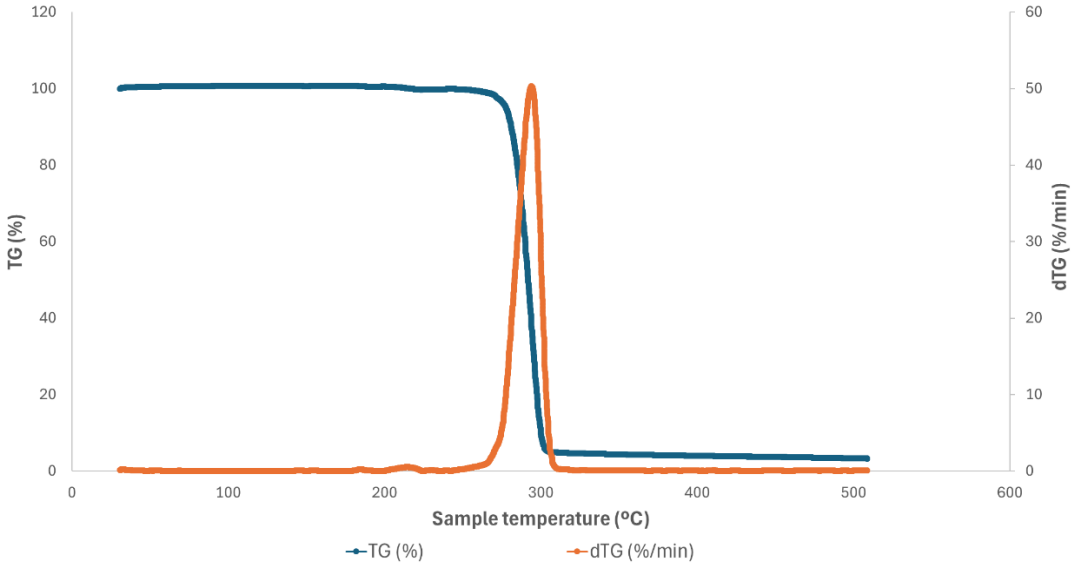

Figure A.10-TGA graphic of sample 2 from Operation 2 with TG (%) and dTG (%/min).

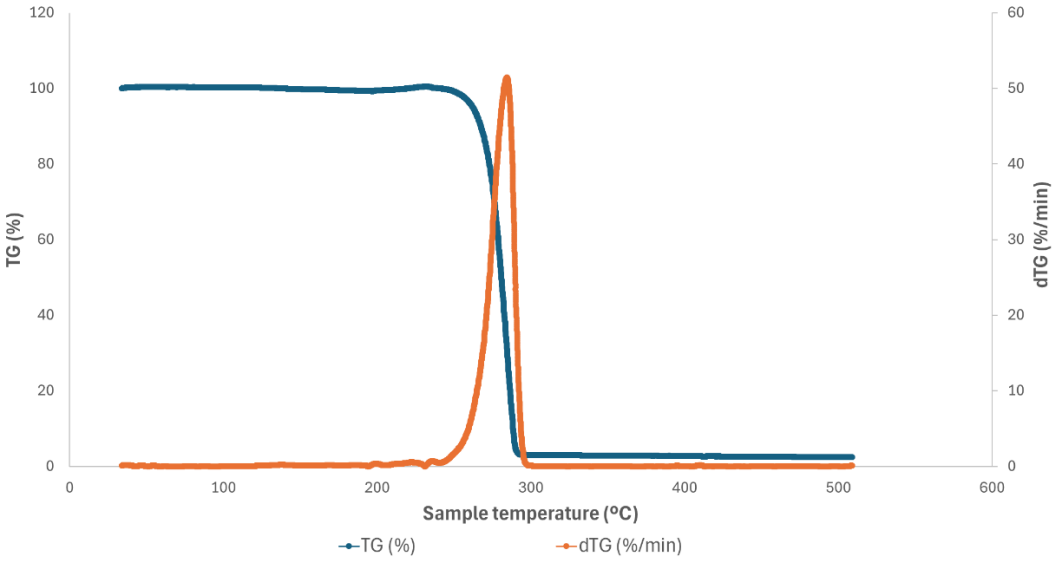

Figure A.11-TGA graphic of sample 1 from Operation 3 with TG (%) and dTG (%/min).

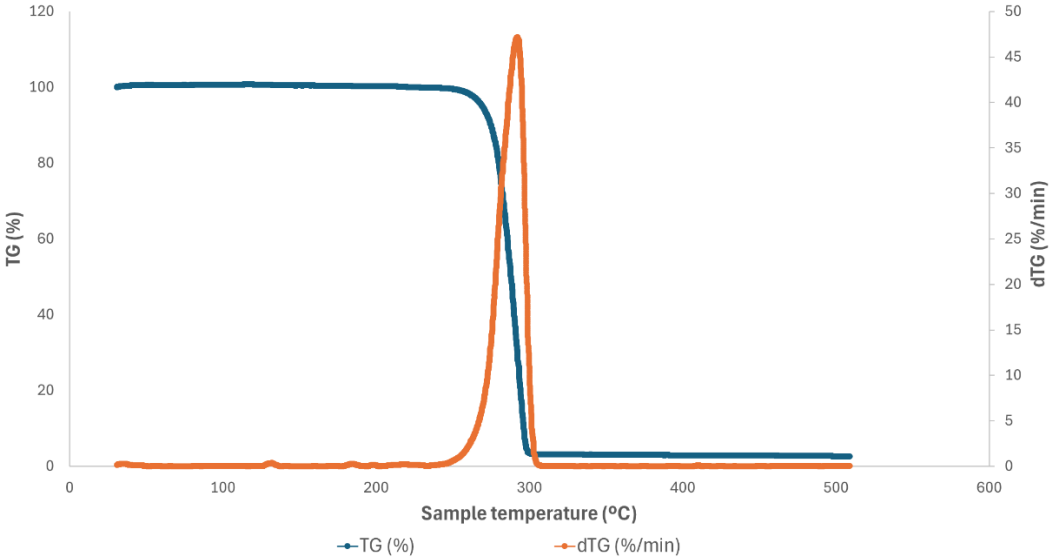

Figure A.12-TGA graphic of sample 2 from Operation 3 with TG (%) and dTG (%/min).

A.3 Graphics from mechanical properties analyses

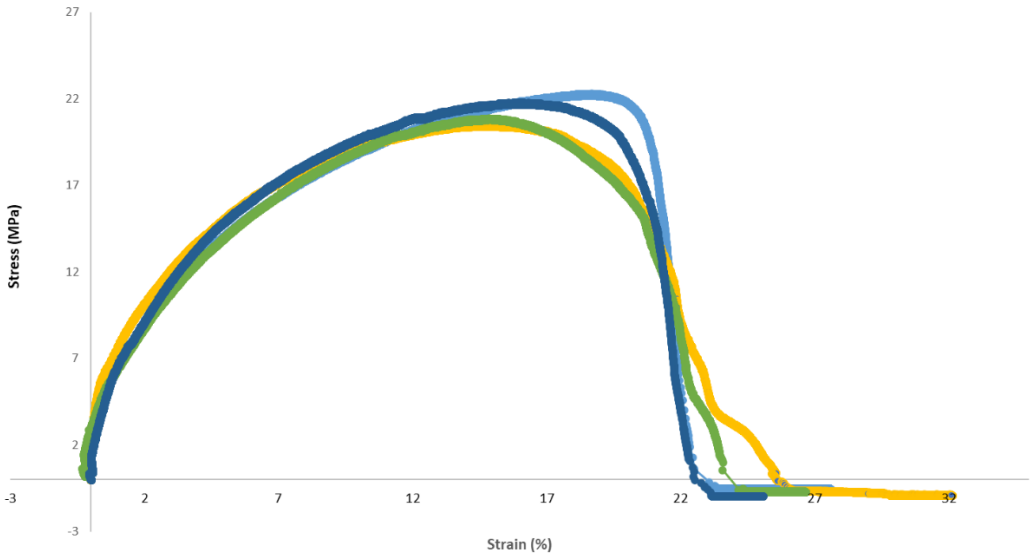

Figure A.13-Grafic of the mechanical properties of the polymer from Operation 1. Each color is a sample.

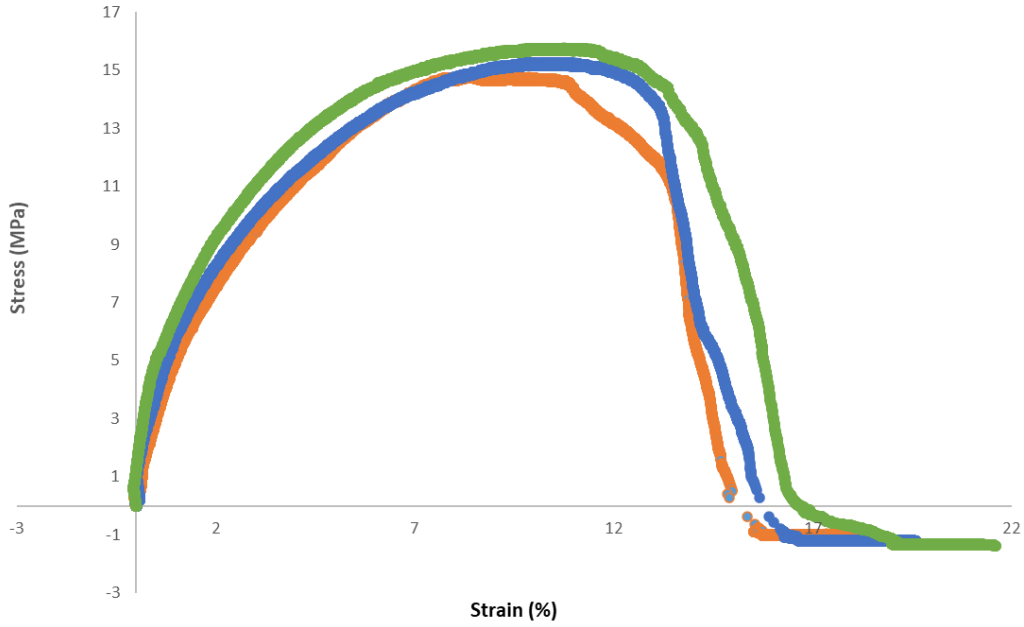

Figure A.14-Grafic of the mechanical properties of the polymer from Operation 2. Each color is a sample.

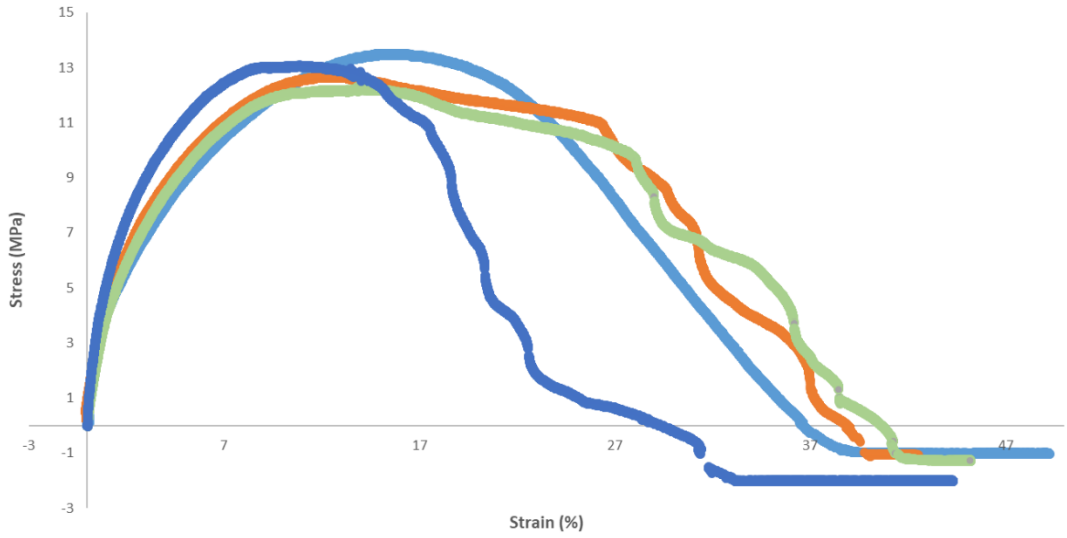

Figure A.15-Grafic of the mechanical properties of the polymer from Operation 3. Each color is a sample.